Eur. Phys. J. A (2015) **51**: 53
DOI 10.1140/epja/i2015-15053-8

THE EUROPEAN PHYSICAL JOURNAL A

Regular Article – Theoretical Physics

Improved chiral nucleon-nucleon potential up to next-to-next-to-next-to-leading order

E. Epelbaum[1,a], H. Krebs[1,b], and U.-G. Meißner[2,3,4,c]

[1] Institut für Theoretische Physik II, Ruhr-Universität Bochum, D-44780 Bochum, Germany
[2] Helmholtz-Institut für Strahlen- und Kernphysik and Bethe Center for Theoretical Physics, Universität Bonn, D-53115 Bonn, Germany
[3] Institut für Kernphysik, Institute for Advanced Simulation, and Jülich Center for Hadron Physics, Forschungszentrum Jülich, D-52425 Jülich, Germany
[4] JARA - High Performance Computing, Forschungszentrum Jülich, D-52425 Jülich, Germany

Received: 15 December 2014 / Revised: 8 April 2015
Published online: 12 May 2015 –
Communicated by H. Wittig

Abstract. We present improved nucleon-nucleon potentials derived in chiral effective field theory up to next-to-next-to-next-to-leading order. We argue that the nonlocal momentum-space regulator employed in the two-nucleon potentials of previous works (Nucl. Phys. A **747**, 362 (2005) and Phys. Rev. C **68**, 041001 (2003)) is not the most efficient choice, in particular since it affects the long-range part of the interaction. We are able to significantly reduce finite-cutoff artefacts by using an appropriate regularization in coordinate space which maintains the analytic structure of the amplitude. The new potentials do not require the additional spectral function regularization employed in (Nucl. Phys. A **747**, 362 (2005)) to cut off the short-range components of the two-pion exchange and make use of the low-energy constants c_i and d_i determined from pion-nucleon scattering without any fine tuning. We discuss in detail the construction of the new potentials and convergence of the chiral expansion for two-nucleon observables. We also employ a simple approach for estimating the theoretical uncertainty in few-nucleon calculations from the truncation of the chiral expansion that replaces previous reliance on cutoff variation.

1 Introduction

In the past decade, we have witnessed impressive progress in the field of low-energy nuclear physics which is, to a large extent, related to exciting theoretical developments. On the one hand, rapidly increasing computational resources and improvements in algorithms make selected nuclear physics observables amenable to numerical simulations in lattice QCD, see ref. [1] for a review article. On the other hand, considerable progress has been achieved towards a quantitative description of nuclear forces within the framework of chiral effective field theory (EFT) initiated in the pioneering work of Weinberg [2]. This approach has been used to derive nuclear forces, defined as kernels of the corresponding dynamical equations, order by order within the EFT expansion, see refs. [3,4] for the first quantitative studies along these lines. The resulting scheme, based on solving the nuclear A-body problem in a Hamiltonian framework with interactions between nucleons tied to QCD via its symmetries, has been developed into a major research field in computational few- and many-body physics and provides nowadays a commonly accepted approach to *ab initio* studies of nuclear structure and reactions [5–9]. In addition to offering a natural explanation for the observed hierarchy of many-body forces, $V_{2N} \gg V_{3N} \gg V_{4N} \ldots$, and allowing for the estimation of the theoretical uncertainty, it is expected to shed light on the long-standing three-nucleon force (3NF) problem, an old but still very current topic in nuclear physics [6,7]. While effects of 3NFs in low-energy nuclear observables are expected to be smaller than the ones of the nucleon-nucleon (NN) force, their inclusion is mandatory at the level of accuracy of today's few- and many-body *ab initio* calculations. However, in spite of decades of effort, the structure of the 3NF is not properly described by the available phenomenological models [6]. Given the very rich spin-momentum structure of the 3NF [10–12], scarcer database for nucleon-deuteron scattering as compared to the NN system and relatively high computational cost of solving the Faddeev equations, further progress in this fields requires substantial input from theory. This provides a strong motivation to study the 3NF within chiral

[a] e-mail: evgeny.epelbaum@rub.de
[b] e-mail: hermann.krebs@rub.de
[c] e-mail: meissner@hiskp.uni-bonn.de

EFT, and this topic is recognized as an important frontier in the field [9, 13, 14]. In particular, the recently formed Low Energy Nuclear Physics International Collaboration (LENPIC) [15] intends to carry out detailed *ab initio* calculations of few- and many-nucleon systems in order to study effects of the 3NF complete through fourth order in the chiral expansion, *i.e.* next-to-next-to-next-to-leading order (N^3LO).

Clearly, looking for fine details of the 3NF, which itself is expected to provide a small correction to the dominant NN force, requires that the NN interaction is known with a sufficiently high accuracy and that one is able to carry out reliable estimation of the theoretical uncertainty. While accurate N^3LO NN potentials have been available for ten years [16, 17], there are certain issues which might become relevant at the accuracy level of the ongoing and planned calculations. First of all, the potentials of ref. [16] employ an additional spectral function regularization (SFR) [18,19] in order to suppress an unphysically strong attraction caused by the very strong short-range components of the subleading two-pion exchange. On the other hand, the available calculations of the 3NF at and beyond the N^3LO level employ the standard dimensional regularization. Introducing the additional SFR on some of the 3NF contributions such as, for example, the so-called ring diagrams, appears to be a nontrivial task. Notice that the potential of ref. [17] avoids the usage of the SFR, but probably at the cost of allowing for a variable functional form of the regulator function for different terms in the interaction, see table F.2 in ref. [20]. Another issue concerns the adopted values of certain pion-nucleon (πN) low-energy constants (LECs) such as especially the c_i's, which accompany the subleading vertices in the πN effective Lagrangian. These LECs govern the strength of the two-pion exchange NN potential and of the long- and intermediate-range 3NFs and should be taken consistently with the πN system. It is well known that some of these LECs and, especially, the LEC c_3 receive significant contributions associated with the intermediate Δ excitation of the nucleon and appear to be numerically large [21]. It was found in ref. [16] that the large empirical values of c_3 would result in generating unphysical deeply bound states in the NN system, so that a reduced value for this LEC has been used in the N^3LO potential of ref. [16]. In the N^3LO potential of ref. [17], the LECs $c_{2,3,4}$ were actually tuned to improve the quality of the fit which resulted, in particular, in the value of c_4 incompatible with the available determinations from the πN system. Perhaps most importantly, the theoretical uncertainty of the calculations due to truncation of the chiral expansion at a given order was so far at best estimated by means of a residual cutoff dependence. As will be argued below, such an approach does not allow for a reliable quantification of the theoretical accuracy.

All these issues clearly call for taking a fresh look at the NN system in chiral EFT. In this work, we introduce a new generation of the chiral N^3LO NN potentials which make use of a local regularization of the pion exchange contributions. The resulting potentials provide an excellent description of low-energy NN scattering observables and the deuteron properties and resolve all the issues mentioned above. In addition, we employ a simple approach for estimating the uncertainty due to truncation of the chiral expansion, which is widely used in chiral perturbation theory and does not rely on cutoff variation, and study in detail the convergence of the chiral expansion for various NN observables.

Our paper is organized as follows. In sect. 2, we discuss the chiral expansion for the NN potential up to N^3LO. The new regularization scheme is introduced in sect. 3, while sect. 4 describes our fit procedure and results for the phase shifts. The cutoff dependence of the obtained predictions is addressed in sect. 5 while our results for the deuteron properties can be found in sect. 6. The theoretical uncertainty of our results is discussed in sect. 7, where we also analyze the convergence of the chiral expansion for various NN scattering observables. Finally, the main findings of our work are summarized in sect. 8.

2 Chiral expansion of the two-nucleon potential

Chiral effective field theory provides a well-defined perturbative expansion for pionic and single-baryon observables as well as for nuclear forces and current operators. In the two-flavor sector we are interested in here, the expansion parameter, denoted as Q, is defined as

$$Q \in \left\{ \frac{p}{\Lambda_b}, \frac{M_\pi}{\Lambda_b} \right\}, \tag{1}$$

where p refers to magnitude of three momenta of external particles, M_π is the pion mass and Λ_b is the breakdown scale of chiral EFT. In the Goldstone boson and single-nucleon sectors, this scale can be naturally expected to be of the order of the ρ-meson mass M_ρ[1]. It was also argued [22] that it cannot be larger than the chiral symmetry breaking scale $\Lambda_\chi = 4\pi F_\pi$, with $F_\pi \simeq 92\,\mathrm{MeV}$ the pion decay constant. On the other hand, in the few-nucleon sector, calculations are usually carried out employing a finite ultraviolet cutoff [23], whose value is typically chosen of the order of $\Lambda \sim 500\,\mathrm{MeV}$. Using soft values of the cutoff may effectively reduce the breakdown scale in the actual calculations. It is, therefore, more appropriate to estimate the breakdown scale of nuclear chiral EFT in a more conservative way rather than by $M_\rho \simeq 770\,\mathrm{MeV}$ or even the chiral symmetry breaking scale $\Lambda_\chi \simeq 1.2\,\mathrm{GeV}$. We will discuss this issue in more detail in sects. 5 and 7.

Up to N^3LO, the NN potential involves contributions from one-, two- and three-pion exchange and contact terms with up to four derivatives which parametrize short-range interactions

$$V = V_{1\pi} + V_{2\pi} + V_{3\pi} + V_{\mathrm{cont}}, \tag{2}$$

[1] In the nucleon sector, one may expect the breakdown scale of the chiral expansion to be lower due to the appearance of the $\Delta(1232)$ resonance. The effects of the intermediate Δ excitations can by systematically taken into account by treating the Δ isobar as an explicit degree of freedom.

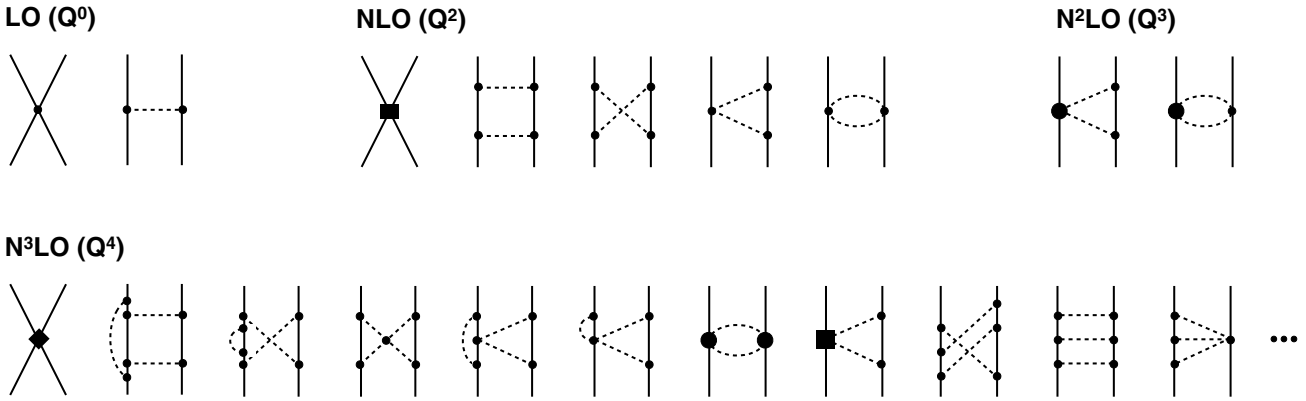

Fig. 1. Chiral expansion of the NN potential up to N^{3}LO. Solid and dashed lines refer to nucleons and pions, respectively. Solid dots denote the vertices from the lowest-order effective Lagrangians $\mathcal{L}_\pi^{(0)}$, $\mathcal{L}_{\pi N}^{(0)}$ and $\mathcal{L}_{NN}^{(0)}$ with the superscript referring to the chiral dimension, for which we use the notation of ref. [5], see this work for explicit expressions. Filled circles refer to vertices from $\mathcal{L}_{\pi N}^{(1)}$ while squares (diamonds) denote vertices from $\mathcal{L}_{\pi N}^{(2)}$ and $\mathcal{L}_{NN}^{(2)}$ ($\mathcal{L}_{NN}^{(4)}$). Only those diagrams are shown which lead to contributions to the potential beyond renormalization of various coupling constants. Only irreducible contributions of various diagrams are taken into account in the potential as explained in the text.

see fig. 1, where the corresponding diagrams are shown. Here and in what follows, we adopt the widely used power counting rules for short-range operators which are based on naive dimensional analysis, see refs. [24–28] for alternative suggestions and refs. [23, 29–32] for a related discussion. We further emphasize that diagrams shown in fig. 1 do actually not correspond to Feynman graphs which provide a graphical representation of the on-shell scattering amplitude. Rather, they should be understood as a schematic visualization of the irreducible parts of the amplitude, *i.e.* those diagrams which do not correspond to iterations of the dynamical equation. For a comprehensive discussion on the various ways to derive energy-independent nuclear potentials and the associated unitary ambiguities see refs. [20, 33–37].

The static one-pion exchange potential (OPEP) is well known and takes the form

$$\begin{aligned} V_{1\pi}^{pp} &= V_{1\pi}^{nn} = V_{1\pi}(M_{\pi^0}), \\ V_{1\pi}^{np} &= -V_{1\pi}(M_{\pi^0}) + 2(-1)^{I+1} V_{1\pi}(M_{\pi^\pm}), \end{aligned} \tag{3}$$

where I denotes the total isospin of the two-nucleon system and

$$V_{1\pi}(M_\pi) = -\frac{g_A^2}{4F_\pi^2}\frac{\vec{\sigma}_1\cdot\vec{q}\,\vec{\sigma}_2\cdot\vec{q}}{q^2+M_\pi^2}\,. \tag{4}$$

Here and in what follows, $\vec{q} = \vec{p}\,' - \vec{p}$ refers to the momentum transfer with $\vec{p}$ and $\vec{p}\,'$ being the initial and final nucleon momenta in the center-of-mass system (cms), while $q \equiv |\vec{q}|$. Further, $\vec{\sigma}_i$ denotes the Pauli spin matrix of nucleon i. Finally, g_A, F_π and $M_{\pi^0}/M_{\pi^\pm}$ denote the axial-vector coupling constant of the nucleon, pion decay constant and neutral/charged pion mass, respectively. Notice that the above expressions include the isospin-breaking (IB) correction due to the different pion masses which is known to be the strongest long-range IB contribution, see refs. [38–43] for more details on the isospin dependence of the NN force. Charge dependence of the pion-nucleon coupling constant is consistent with zero [44] and for this reason will not be taken into account in the present work. The form of the longest-range NN force specified above coincides with the one employed in the Nijmegen partial wave analysis (NPWA) [45] which we use as input for tuning the short-range interactions. Relativistic corrections to the OPEP will be discussed at the end of this section.

The chiral expansion of the two-pion exchange potential (TPEP) starts at next-to-leading order (NLO) which corresponds to the chiral order Q^2. Using the decomposition of the momentum-space TPEP

$$\begin{aligned} V_{2\pi} = {} & V_C + \boldsymbol{\tau}_1\cdot\boldsymbol{\tau}_2\, W_C \\ & + [V_S + \boldsymbol{\tau}_1\cdot\boldsymbol{\tau}_2\, W_S]\ \vec{\sigma}_1\cdot\vec{\sigma}_2 \\ & + [V_T + \boldsymbol{\tau}_1\cdot\boldsymbol{\tau}_2\, W_T]\ \vec{\sigma}_1\cdot\vec{q}\,\vec{\sigma}_2\cdot\vec{q} \\ & + [V_{LS} + \boldsymbol{\tau}_1\cdot\boldsymbol{\tau}_2\, W_{LS}]\ i(\vec{\sigma}_1+\vec{\sigma}_2)\cdot(\vec{q}\times\vec{k}\,), \end{aligned} \tag{5}$$

where $\vec{k} = (\vec{p}+\vec{p}\,')/2$, $\boldsymbol{\tau}_i$ denote the isospin Pauli matrices associated with the nucleon i, while $V_{C,S,T,LS}$ and $W_{C,S,T,LS}$ are scalar functions which depend on the nucleon momenta, the order-Q^2 contributions take the form

$$\begin{aligned} W_C^{(2)} &= -\frac{L(q)}{384\pi^2F_\pi^4}\Bigg[4M_\pi^2(5g_A^4-4g_A^2-1) \\ &\qquad +q^2(23g_A^4-10g_A^2-1)+\frac{48g_A^4M_\pi^4}{4M_\pi^2+q^2}\Bigg], \\ V_T^{(2)} &= -\frac{1}{q^2}V_S^{(2)} = -\frac{3g_A^4}{64\pi^2F_\pi^4}\,L(q), \\ V_C^{(2)} &= V_{LS}^{(2)} = W_S^{(2)} = W_T^{(2)} = W_{LS}^{(2)} = 0. \end{aligned} \tag{6}$$

The loop function $L(q)$ is defined in dimensional regularization (DR) via

$$L(q) = \frac{\sqrt{4M_\pi^2+q^2}}{q}\ln\frac{\sqrt{4M_\pi^2+q^2}+q}{2M_\pi}\,. \tag{7}$$

Notice that we only list here nonpolynomial in momenta contributions while all polynomial terms are absorbed into contact interactions which will be discussed below.

The corrections at order Q^3 giving rise to the subleading TPEP have the form

$$\begin{aligned}
V_C^{(3)} &= -\frac{3g_A^2}{16\pi F_\pi^4}\big[2M_\pi^2(2c_1-c_3)-c_3q^2\big](2M_\pi^2+q^2)A(q),\\
W_T^{(3)} &= -\frac{1}{q^2}W_S^{(3)} = -\frac{g_A^2}{32\pi F_\pi^4}\,c_4(4M_\pi^2+q^2)A(q),\\
V_S^{(3)} &= V_T^{(3)} = V_{LS}^{(3)} = W_C^{(3)} = W_{LS}^{(3)} = 0,
\end{aligned} \tag{8}$$

where c_i are LECs associated with the subleading $\pi\pi NN$ vertices from $\mathcal{L}_{\pi N}^{(1)}$ and the loop function $A(q)$ is given in DR by

$$A(q) = \frac{1}{2q}\arctan\frac{q}{2M_\pi}\,. \tag{9}$$

At order Q^4, *i.e.* N^{3}LO, one encounters further corrections to the TPEP emerging from the various one- and two-loop diagrams which have been calculated in ref. [46]. The contributions of the one-loop "bubble" diagrams to the TPEP take a particularly simple form

$$\begin{aligned}
V_C^{(4)} &= \frac{3}{16\pi^2F_\pi^4}\,L(q)\left\{\left[\frac{c_2}{6}(4M_\pi^2+q^2)+c_3(2M_\pi^2+q^2)\right.\right.\\
&\quad\left.\left.-4c_1M_\pi^2\right]^2+\frac{c_2^2}{45}(4M_\pi^2+q^2)^2\right\}\\
W_T^{(4)} &= -\frac{1}{q^2}W_S^{(4)} = \frac{c_4^2}{96\pi^2F_\pi^4}(4M_\pi^2+q^2)\,L(q).
\end{aligned} \tag{10}$$

The remaining contributions from one- and two-loop diagrams can be most conveniently written using the (subtracted) spectral representation of the TPEP

$$\begin{aligned}
V_{C,S}(q) &= -\frac{2q^6}{\pi}\int_{2M_\pi}^\infty \mathrm{d}\mu\frac{\rho_{C,S}(\mu)}{\mu^5(\mu^2+q^2)}\,,\\
V_T(q) &= \frac{2q^4}{\pi}\int_{2M_\pi}^\infty \mathrm{d}\mu\frac{\rho_T(\mu)}{\mu^3(\mu^2+q^2)}\,,\\
W_{C,S}(q) &= -\frac{2q^6}{\pi}\int_{2M_\pi}^\infty \mathrm{d}\mu\frac{\eta_{C,S}(\mu)}{\mu^5(\mu^2+q^2)}\,,\\
W_T(q) &= \frac{2q^4}{\pi}\int_{2M_\pi}^\infty \mathrm{d}\mu\frac{\eta_T(\mu)}{\mu^3(\mu^2+q^2)}\,,
\end{aligned} \tag{11}$$

where ρ_i and η_i denote the corresponding spectral functions which are related to the potential via $\rho_i(\mu) = \mathrm{Im}\,V_i(i\mu)$, $\eta_i(\mu) = \mathrm{Im}\,W_i(i\mu)$. For the spectral functions $\rho_i(\mu)$ $(\eta_i(\mu))$ one finds [46]:

$$\begin{aligned}
\rho_C^{(4)}(\mu) &= -\frac{3g_A^4(\mu^2-2M_\pi^2)}{\pi\mu(4F_\pi)^6}\\
&\quad\times\left\{(M_\pi^2-2\mu^2)\left[2M_\pi+\frac{2M_\pi^2-\mu^2}{2\mu}\ln\frac{\mu+2M_\pi}{\mu-2M_\pi}\right]\right.\\
&\quad\left.+4g_A^2M_\pi(2M_\pi^2-\mu^2)\right\},\\
\eta_S^{(4)}(\mu) &= \mu^2\eta_T^{(4)}(\mu) = -\frac{g_A^4(\mu^2-4M_\pi^2)}{\pi(4F_\pi)^6}\,\left\{\left(M_\pi^2-\frac{\mu^2}{4}\right)\right.\\
&\quad\left.\times\ln\frac{\mu+2M_\pi}{\mu-2M_\pi}+(1+2g_A^2)\mu M_\pi\right\},\\
\rho_S^{(4)}(\mu) &= \mu^2\rho_T^{(4)}(\mu) = -\left\{\frac{g_A^2r^3\mu}{8F_\pi^4\pi}(\bar d_{14}-\bar d_{15})\right.\\
&\quad\left.-\frac{2g_A^6\mu r^3}{(8\pi F_\pi^2)^3}\left[\frac{1}{9}-J_1+J_2\right]\right\},\\
\eta_C^{(4)}(\mu) &= \left\{\frac{rt^2}{24F_\pi^4\mu\pi}\left[2(g_A^2-1)r^2-3g_A^2t^2\right](\bar d_1+\bar d_2)\right.\\
&\quad+\frac{r^3}{60F_\pi^4\mu\pi}\left[6(g_A^2-1)r^2-5g_A^2t^2\right]\bar d_3\\
&\quad-\frac{rM_\pi^2}{6F_\pi^4\mu\pi}\left[2(g_A^2-1)r^2-3g_A^2t^2\right]\bar d_5\\
&\quad-\frac{1}{92160F_\pi^6\mu^2\pi^3}\Big[-320(1+2g_A^2)^2M_\pi^6\\
&\quad+240(1+6g_A^2+8g_A^4)M_\pi^4\mu^2\\
&\quad-60g_A^2(8+15g_A^2)M_\pi^2\mu^4+(-4+29g_A^2\\
&\quad\left.+122g_A^4+3g_A^6)\mu^6\Big]\ln\frac{2r+\mu}{2M_\pi}-\frac{r}{2700\mu(8\pi F_\pi^2)^3}\right.\\
&\quad\times\Big[-16(171+2g_A^2(1+g_A^2)(327+49g_A^2))M_\pi^4\\
&\quad+4(-73+1748g_A^2+2549g_A^4+726g_A^6)M_\pi^2\mu^2\\
&\quad-(-64+389g_A^2+1782g_A^4+1093g_A^6)\mu^4\Big]\\
&\quad\left.+\frac{2r}{3\mu(8\pi F_\pi^2)^3}\Big[g_A^6t^4J_1-2g_A^4(2g_A^2-1)r^2t^2J_2\Big]\right\},
\end{aligned} \tag{12}$$

where we have introduced the abbreviations

$$r = \frac{1}{2}\sqrt{\mu^2-4M_\pi^2}\,,\qquad t = \sqrt{\mu^2-2M_\pi^2}\,, \tag{13}$$

and

$$\begin{aligned}
J_1 &= \int_0^1 \mathrm{d}x\left\{\frac{M_\pi^2}{r^2x^2}-\left(1+\frac{M_\pi^2}{r^2x^2}\right)^{3/2}\right.\\
&\quad\left.\times\ln\frac{rx+\sqrt{M_\pi^2+r^2x^2}}{M_\pi}\right\},\\
J_2 &= \int_0^1 \mathrm{d}x\,x^2\left\{\frac{M_\pi^2}{r^2x^2}-\left(1+\frac{M_\pi^2}{r^2x^2}\right)^{3/2}\right.\\
&\quad\left.\times\ln\frac{rx+\sqrt{M_\pi^2+r^2x^2}}{M_\pi}\right\}.
\end{aligned} \tag{14}$$

Here and in what follows, we use the scale-independent LECs $\bar{d}_1$, $\bar{d}_2$, $\bar{d}_3$, $\bar{d}_5$, $\bar{d}_{14}$ and $\bar{d}_{15}$ defined in [47]. One also has to account for relativistic corrections to the TPEP which will be discussed at the end of this section.

The short-range part of the chiral potential involves in the isospin limit two derivative-less interactions contributing at leading order (LO), seven terms involving two derivatives at next-to-leading order (NLO) and fifteen terms involving four derivatives at N^{3}LO. For isospin-breaking contact interactions, we employ here only the leading derivative-less terms which give rise to charge independence and charge symmetry breaking in the $^1S_0$ NN phase shift. Notice that at N^{3}LO, one, strictly speaking, also needs to take into account IB TPEP as well as the $\pi\gamma$-exchange potential. Given that we use the NPWA rather than experimental data as input to determine various LECs accompanying short-range interactions, we employ here the same treatment of IB effects as used by the Nijmegen group. Specifically, the only sources of (finite-range) IB contributions to the NN force are given by the OPEP, see eq. (3) and the two derivative-less IB contact interactions. This is also exactly the same procedure as the one employed in our analysis reported in ref. [16]. The contact interactions used in the present work yield the following contributions to the NN potential in the partial-wave basis

$$
\begin{aligned}
\langle {}^1S_0,\,\mathrm{np}|V^{\mathrm{np}}_{\mathrm{cont}}|{}^1S_0,\,\mathrm{np}\rangle &= \tilde{C}^{\mathrm{np}}_{1S0} + C_{1S0}(p^2+p'^2) \\
&\quad + D^1_{1S0}\,p^2\,p'^2 + D^2_{1S0}(p^4+p'^4), \\
\langle {}^1S_0,\,\mathrm{pp}|V^{\mathrm{pp}}_{\mathrm{cont}}|{}^1S_0,\,\mathrm{pp}\rangle &= \tilde{C}^{\mathrm{pp}}_{1S0} + C_{1S0}(p^2+p'^2) \\
&\quad + D^1_{1S0}\,p^2\,p'^2 + D^2_{1S0}(p^4+p'^4), \\
\langle {}^1S_0,\,\mathrm{nn}|V^{\mathrm{nn}}_{\mathrm{cont}}|{}^1S_0,\,\mathrm{nn}\rangle &= \tilde{C}^{\mathrm{nn}}_{1S0} + C_{1S0}(p^2+p'^2) \\
&\quad + D^1_{1S0}\,p^2\,p'^2 + D^2_{1S0}(p^4+p'^4), \\
\langle {}^3S_1|V_{\mathrm{cont}}|{}^3S_1\rangle &= \tilde{C}_{3S1} + C_{3S1}(p^2+p'^2) \\
&\quad + D^1_{3S1}\,p^2\,p'^2 + D^2_{3S1}(p^4+p'^4), \\
\langle {}^1P_1|V_{\mathrm{cont}}|{}^1P_1\rangle &= C_{1P1}\,p\,p' + D_{1P1}\,p\,p'(p^2+p'^2), \\
\langle {}^3P_1|V_{\mathrm{cont}}|{}^3P_1\rangle &= C_{3P1}\,p\,p' + D_{3P1}\,p\,p'(p^2\ +p'^2), \\
\langle {}^3P_0|V_{\mathrm{cont}}|{}^3P_0\rangle &= C_{3P0}\,p\,p' + D_{3P0}\,p\,p'(p^2+p'^2), \\
\langle {}^3P_2|V_{\mathrm{cont}}|{}^3P_2\rangle &= C_{3P2}\,p\,p' + D_{3P2}\,p\,p'(p^2+p'^2), \\
\langle {}^1D_2|V_{\mathrm{cont}}|{}^1D_2\rangle &= D_{1D2}\,p^2\,p'^2, \\
\langle {}^3D_2|V_{\mathrm{cont}}|{}^3D_2\rangle &= D_{3D2}\,p^2\,p'^2, \\
\langle {}^3D_1|V_{\mathrm{cont}}|{}^3D_1\rangle &= D_{3D1}\,p^2\,p'^2, \\
\langle {}^3D_3|V_{\mathrm{cont}}|{}^3D_3\rangle &= D_{3D3}\,p^2\,p'^2, \\
\langle {}^3S_1|V_{\mathrm{cont}}|{}^3D_1\rangle &= C_{3D1-3S1}\,p^2 + D^1_{3D1-3S1}\,p^2\,p'^2 \\
&\quad + D^2_{3D1-3S1}\,p^4, \\
\langle {}^3D_1|V_{\mathrm{cont}}|{}^3S_1\rangle &= C_{3D1-3S1}\,p'^2 + D^1_{3D1-3S1}\,p^2\,p'^2 \\
&\quad + D^2_{3D1-3S1}\,p'^4, \\
\langle {}^3P_2|V_{\mathrm{cont}}|{}^3F_2\rangle &= D_{3F2-3P2}\,p^3\,p', \\
\langle {}^3F_2|V_{\mathrm{cont}}|{}^3P_2\rangle &= D_{3F2-3P2}\,p\,p'^3, \qquad (15)
\end{aligned}
$$

where $\tilde{C}_i$, $\tilde{C}^{\mathrm{np}}_i$, $\tilde{C}^{\mathrm{pp}}_i$, $\tilde{C}^{\mathrm{nn}}_i$, C_i and D_i denote the corresponding LECs. The relation between these LECs and the ones corresponding to the operator form of the short-range potential can be found in eq. (2.6) of ref. [16]. Notice further that we do not show explicitly the pion mass dependence of various contact interactions.

Finally, let us discuss the relativistic corrections to the potential which according to our power counting scheme start to contribute at N^{3}LO. Notice that following ref. [48], we treat the nucleon mass as a heavier scale as compared with the breakdown scale Λ_b by counting $Q/m_N \sim Q^2/\Lambda_b^2$. The relativistic corrections are scheme-dependent or, more precisely, depend on the employed form of the dynamical equation and the choice of unitary transformations as explained in detail in ref. [49]. Contrary to the static N^{3}LO contributions, the results for the $1/m_N^2$-corrections to the OPEP and $1/m_N$-corrections to the TPEP are not uniquely determined by the renormalizability requirement of the nuclear forces [50] and depend on two arbitrary parameters, called $\bar{\beta}_{8,9}$ in that work, which correspond to the unitary ambiguity of the potential and are related to the parameters μ and ν of ref. [49] via

$$
\begin{aligned}
\mu &= 4\bar{\beta}_9 + 1, \\
\nu &= 2\bar{\beta}_8. \qquad (16)
\end{aligned}
$$

Here and in what follows, we employ the "minimal nonlocality" choice of the potential corresponding to setting $\mu = 0$ and $\nu = 1/2$ or, equivalently, $\bar{\beta}_8 = 1/4$, $\bar{\beta}_9 = -1/4$ (see footnote[2]). This particular choice implies that the only $1/m_N^2$-corrections to the OPEP stem from accounting for the relativistic normalization of the nucleon field operators. Using the relativistic Schrödinger equation for NN scattering of the form

$$
\left[2\sqrt{p^2+m_N^2}+V\right]\Psi = 2\sqrt{k^2+m_N^2}\Psi, \qquad (17)
$$

where $m_N = m_p$ for the proton-proton (pp), $m_N = m_n$ for the neutron-neutron (nn) and $m_N = 2m_pm_n/(m_p + m_n)$ for the neutron-proton (np) case and k denotes the momentum corresponding to the energy eigenvalue E, the full nonstatic expression for the OPEP takes the form

$$
\begin{aligned}
V_{1\pi} &= \frac{m_N}{E_0}\,V^{\mathrm{static}}_{1\pi}\,\frac{m_N}{E_0} \\
&= \left(1-\frac{p^2+p'^2}{2m_N^2}+\mathcal{O}(m_N^{-4})\right)V^{\mathrm{static}}_{1\pi}\,, \qquad (18)
\end{aligned}
$$

where $E_0 = \sqrt{p^2+m_N^2}$ is an operator. Notice that here and in what follows, we use the notation $p \equiv |\vec{p}|$, $p' \equiv |\vec{p}\,'|$ and $q \equiv |\vec{q}|$. The corresponding $1/m_N$-corrections to the

[2] We correct here a misprint in eq. (4.24) of ref. [50], where the "minimal nonlocality" choice was specified by $\bar{\beta}_8 = 1/4$, $\bar{\beta}_9 = 0$.

TPEP read [49][3]

$$
\begin{aligned}
V_C^{(4)} &= \frac{3g_A^4}{512\pi m_N F_\pi^4}\left\{\frac{2M_\pi^5}{4M_\pi^2+q^2} - 3(4M_\pi^4 - q^4)A(q)\right\},\\
W_C^{(4)} &= \frac{g_A^2}{128\pi m_N F_\pi^4}\left\{\frac{3g_A^2 M_\pi^5}{4M_\pi^2+q^2} - \left[4M_\pi^2+2q^2\right.\right.\\
&\quad \left.\left. -g_A^2\left(7M_\pi^2+\frac{9}{2}q^2\right)\right](2M_\pi^2+q^2)A(q)\right\},\\
V_T^{(4)} &= -\frac{1}{q^2}V_S^{(4)} = \frac{9g_A^4}{512\pi m_N F_\pi^4}\left(4M_\pi^2+\frac{3}{2}q^2\right)A(q),\\
W_T^{(4)} &= -\frac{1}{q^2}W_S^{(4)} = -\frac{g_A^2}{256\pi m_N F_\pi^4}\left[8M_\pi^2+2q^2\right.\\
&\quad \left. -g_A^2\left(4M_\pi^2+\frac{3}{2}q^2\right)\right]A(q),\\
V_{LS}^{(4)} &= -\frac{3g_A^4}{64\pi m_N F_\pi^4}(2M_\pi^2+q^2)A(q),\\
W_{LS}^{(4)} &= -\frac{g_A^2(1-g_A^2)}{64\pi m_N F_\pi^4}(4M_\pi^2+q^2)A(q).
\end{aligned}
\tag{19}
$$

It is customary to rewrite the relativistic Schrödinger equation (17) in the equivalent nonrelativistic form [49]

$$
\left[\frac{p^2}{m_N}+\tilde{V}\right]\Psi' = \frac{k^2}{m_N}\Psi', \tag{20}
$$

where the potential operator $\tilde{V}$ is given by

$$
\tilde{V} = \left\{\frac{\sqrt{p^2+m_N^2}}{2m_N},\, V\right\} + \frac{V^2}{4m_N}\,, \tag{21}
$$

and $\{,\}$ denotes the anti-commutator. This implies, in particular, that the $1/m_N$-corrections to the TPEP receive further contributions induced by the second term in the right-hand side of the above equation, $V_{1\pi}^2/(4m_N)$, which have the form

$$
\begin{aligned}
\delta V_C^{(4)} &= \frac{3g_A^4}{512\pi m_N F_\pi^4}(2M_\pi^2+q^2)^2 A(q),\\
\delta W_C^{(4)} &= -\frac{g_A^4}{256\pi m_N F_\pi^4}(2M_\pi^2+q^2)^2 A(q),\\
\delta V_T^{(4)} &= -\frac{1}{q^2}\delta V_S^{(4)} = -\frac{3g_A^4}{1024\pi m_N F_\pi^4}(4M_\pi^2+q^2)A(q),\\
\delta W_T^{(4)} &= -\frac{1}{q^2}\delta W_S^{(4)} = \frac{g_A^4}{512\pi m_N F_\pi^4}(4M_\pi^2+q^2)A(q),
\end{aligned}
\tag{22}
$$

and need to be added to the expressions in eq. (19). It is this form of the Schrödinger equation which was used in the NPWA and is employed in the present analysis. We refer the reader to appendix A for more details on the kinematics and notations. To summarize, the relativistic corrections to the NN potential at N^{3}LO in the cms employed in the present work consist of:

- $1/m_N$-corrections to the static TPEP according to eqs. (19) and (22);
- $\mathcal{O}(m_N^{-2})$-corrections to the static OPEP and the resulting TPEP according to eqs. (18) and (21),

$$
\left\{\frac{m_N}{2E_0},\, V_{1\pi}^{\rm static}+V_{2\pi}\right\} - (V_{1\pi}^{\rm static}+V_{2\pi}). \tag{23}
$$

  This particular choice is appropriate at the order we are working and is well suited for the local regularization of the long-range potentials employed in our analysis, see the next section for more details. Notice that the relativistic corrections to the contact interactions in the cms have the same form as the static terms and thus need not to be considered separately.

We emphasize that we also included the leading $1/m_N$-corrections emerging from triangle two-pion exchange diagrams involving subleading πN vertices, *i.e.* proportional to c_i. The corresponding expressions are not affected by unitary ambiguity of the potential and can be found in ref. [46]. While these contributions appear nominally at next-to-next-to-next-to-next-to-leading order in the chiral expansion within the employed power counting scheme, the resulting potentials are known to be rather strong, presumably due to the LECs $c_{2,3,4}$ being numerically large. We have checked that neglecting those terms does not substantially affect the quality of the fits but would result in a smaller range of cutoffs. Finally, notice that similar to refs. [16,17], we do not explicitly include the leading three-pion exchange potential which is known to be weak.

3 Regularization

Nuclear potentials derived in chiral EFT generate ultraviolet (UV) divergences once substituted into the Lippmann-Schwinger (LS) equation. The appearance of UV divergences in loop diagrams is an intrinsic feature of any EFT which can be traced back to the derivative expansion of the effective Lagrangian. While perturbative calculations of, *e.g.*, pion-pion or pion-nucleon scattering within chiral perturbation theory are usually organized in such a way that *all* UV divergences at a given order are absorbable into redefinition of the available LECs, the situation is different for nucleon-nucleon scattering described in terms of nonperturbative solution of the LS equation. While it is possible to formulate a *renormalizable* approach to NN scattering with nonperturbative treatment of the OPEP [31, 51, 52], a much simpler and commonly adopted way to renormalize the LS equation is based on introducing a finite UV cutoff. (Implicit) renormalization of the NN amplitude is then achieved by tuning the (bare) LECs accompanying the contact interactions

[3] Notice that there are misprints in eq. (2.23) of ref. [16] for $V_T^{(4)}$ and $W_{T,S}^{(4)}$.

to experimental data or phase shifts. One advantage of such an approach, beyond its simplicity, is the ability to combine the resulting nuclear potentials with the available few- and many-body machinery which allows one to access observables beyond the NN system. The obvious disadvantage compared to the renormalizable framework suggested in ref. [31] is the appearance of finite-cutoff artefacts as manifested, *e.g.*, in a residual cutoff dependence of nuclear observables. This feature is unavoidable in calculations within such an approach (unless one is able to subtract *all* divergent integrals generated by iterations of the chiral potentials in the LS equation). As a consequence, the UV momentum-space cutoff Λ has to be kept finite and (ideally) of the order of the pertinent breakdown scale in the problem [23, 29, 30, 53].

In practice, one is rather limited with respect to the range of cutoff values since choosing $\Lambda \sim M_\rho$ or larger was already found to result in spurious deeply bound states [16]. While such unphysical deeply bound state do not affect low-energy observables, they do drastically complicate applications to three- and more-nucleon systems. For this reason, ref. [16] has employed the cutoff range of $\Lambda = 450 \ldots 600\,\mathrm{MeV}$ while the Idaho $\mathrm{N^3LO}$ potential is available for two cutoff values only, namely $\Lambda = 500\,\mathrm{MeV}$ and $\Lambda = 600\,\mathrm{MeV}$ [17, 20]. We further emphasize that lattice spacings employed in recent nuclear lattice simulations of refs. [54–59] correspond to even smaller cutoff values.

Given the relatively low values of Λ, it is clearly desirable, in order to increase the accuracy and applicability range of nuclear chiral EFT, to reduce the amount of finite-cutoff artefacts, see ref. [60] for a recent lattice EFT work in a similar spirit, or at least to employ regularization which avoids introducing unnecessary artefacts. In the following, we will argue that the momentum-space regularization used in the $\mathrm{N^3LO}$ potentials of refs. [16, 17] does induce certain kinds of artefacts which can be easily avoided by carrying out regularization in coordinate space as used recently in the construction of the local chiral NN potentials up to next-to-next-to-leading order ($\mathrm{N^2LO}$) [61, 62].

Chiral nuclear forces involve generally two distinct kinds of contributions: first, at large distances the potential is governed by contributions emerging from pion exchanges which are unambiguously[4] determined by the chiral symmetry of QCD and experimental information on the pion-nucleon system needed to pin down the relevant LECs. Secondly, the short-range part of the potential is parametrized by all possible contact interactions with increasing number of derivatives. It is desirable to introduce regularization in such a way that the long-range part of the interaction including especially the OPEP, which is responsible for left-hand cuts in the partial-wave scattering amplitude as visualized in fig. 2 and thus governs near-threshold energy behavior of the S-matrix, is not affected by the regulator. Notice that the near-threshold left-hand singularities of the amplitude can be tested, *e.g.*, via the low-energy theorems [30, 63].

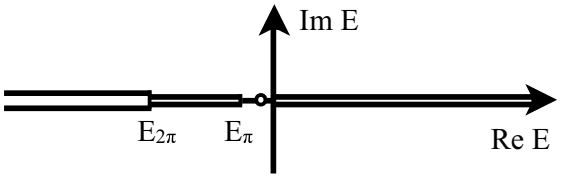

Fig. 2. Singularity structure of the partial-wave two-nucleon scattering amplitude in the complex energy plane. The solid dot indicates the position of the S-wave (virtual) bound state. Elastic unitarity is satisfied on the right-hand cut, also called unitarity cut. Left-hand cuts are caused by exchange processes in the potential. The first and second left-hand cuts due to one- and two-pion exchange start at laboratory energy of $E_\pi = -M_\pi^2/(2m_N) \sim 10\,\mathrm{MeV}$ and $E_{2\pi} = -2M_\pi^2/m_N \sim 40\,\mathrm{MeV}$, respectively.

The standard implementation of the regulator used, *e.g.*, in refs. [16, 17] is as follows:

$$V(\vec{p}\,',\vec{p}) \to V_{\mathrm{reg}}(\vec{p}\,',\vec{p}) = V(\vec{p}\,',\vec{p}) \exp\left(-\frac{p'^m + p^m}{\Lambda^m}\right), \tag{24}$$

where the power m is chosen sufficiently large in order that the cutoff artefacts $V(\vec{p}\,',\vec{p}) \times \mathcal{O}((Q/\Lambda)^m)$ are beyond the chiral order one is working at. Specifically, ref. [16] used $m = 6$ while ref. [17] employed different powers $m \leq 6$ for different terms in the potential, presumably in order to optimize the quality of the fit. It is clear that the multiplicative regulator introduced above leads to distortions of the analytic structure of the partial-wave amplitude near threshold as it affects the discontinuity across the left-hand cuts, see also refs. [64, 65] for recent studies of NN scattering which explicitly exploit the analytic structure of the amplitude. While such distortions are small if Λ can be chosen sufficiently large, they can lead to sizable effects for the commonly adopted choices of $\Lambda \sim 500\,\mathrm{MeV}$. It is easy to avoid this unpleasant feature by exploiting the fact that long-range potentials derived in chiral EFT are nearly local, *i.e.* depend only on momentum transfer $\vec{q}$. In fact, the only source of nonlocality is given by relativistic corrections which, in the power counting scheme we are using, start to appear at $\mathrm{N^3LO}$, see the previous section. The feature of locality naturally suggests to apply regularization in coordinate space similar to what was done in refs. [61, 62] by cutting off *short-range* parts of the pion-exchange potentials, for which chiral expansion does not converge, see ref. [66] for a related discussion:

$$V_{\text{long-range}}(\vec{r}) \to V^{\mathrm{reg}}_{\text{long-range}}(\vec{r}) = V_{\text{long-range}}(\vec{r}) f\left(\frac{r}{R}\right), \tag{25}$$

where the regulator function $f(x)$ is chosen such that its value goes to 0 (1) sufficiently fast for $x \to 0$ ($x \gg 1$). It is instructive to write this

[4] Strictly speaking, even the long-range tail of the potential is scheme-dependent as it can be affected by unitary transformations. Notice, however, that unitary ambiguity of the chiral nuclear forces was found to be strongly reduced in the static limit if one demands that the corresponding potentials are renormalizable [36].

regularization in momentum space,

$$V(\vec{q}) \to V^{\rm reg}(\vec{q}) = V(\vec{q}) - \int \frac{{\rm d}^3 l}{(2\pi)^3} V(\vec{l})\, {\rm FT}_{\vec{q}-\vec{l}}[1-f], \tag{26}$$

where FT stays for the Fourier-Transform. Given that FT$[1-f]$ is a short-range operator, the second term in the right-hand side of the above equation does not induce any long-range contributions. This is in contrast to the procedure specified in eq. (24), where long-range terms are induced by regularization (albeit suppressed by inverse powers of the cutoff Λ). Notice further that the suggested regularization is qualitatively similar to the well-known Pauli-Villars regularization.

As will be shown in the next section, the above choice of the regulator makes the additional SFR of the pion exchange contributions obsolete. This is a particularly welcome feature in view of the fact that the expressions for the three-nucleon force at N^{3}LO [50,67,68] are only available in the framework of DR which corresponds to choosing an infinitely large cutoff in the spectral function representation. Notice further that recent calculations of the three-nucleon force beyond N^{3}LO [10, 69] are also carried out in the framework of DR. The SFR was originally introduced in refs. [18, 19] as an attempt to avoid unnaturally strong attraction generated by the subleading TPEP in the isoscalar central channel [33] caused by short-range components in the spectral representation. The SFR framework was used to construct the N^{3}LO potential of ref. [16]. Notice, however, that in spite of employing the SFR, it was necessary to set the LEC c_3, which governs the isoscalar part of the N^{2}LO TPEP, to its lowest in magnitude value still compatible with πN scattering in order to avoid the appearance of deeply bound states.

We are now in the position to specify the regulator function $f(r/R)$, for which the choice $f(r/R) = 1 - \exp(-(r/R)^4)$ was adopted in refs. [61,62]. Given that DR expressions for TPEP at N^{2}LO behave at short distances as $1/r^6$, such a regulator is insufficient to make the DR potential nonsingular and can only be used in combination with the SFR which makes the TPEP less singular. Notice further that such a regulator induces oscillations in momentum-space matrix elements of the potential $V(\vec{q})$ for large values of q which may represent a considerable complication for numerical applications. In order to avoid this unpleasant feature, the regulator function can be chosen in the form

$$f\left(\frac{r}{R}\right) = \left[1 - \exp\left(-\frac{r^2}{R^2}\right)\right]^n, \tag{27}$$

where the exponent n has to be taken sufficiently large. It is necessary to choose $n = 4$ or larger in order to make the regularized expressions for the DR TPEP at N^{3}LO vanishing in the origin, but we found that larger values of n lead to more stable numerical results when doing calculations in momentum space[5]. Here and in what follows, we make the choice $n = 6$. For contact interactions, we employ the standard nonlocal regulator specified in eq. (24) and set $m = 2$ so that the regulator is again of a Gaussian type. In order to have a single cutoff scale, we will relate the coordinate- and momentum-space cutoffs R and Λ by setting $\Lambda = 2R^{-1}$ motivated by the relation ${\rm FT}_q[\exp(-r^2/R^2)] \propto \exp(-q^2R^2/4)$. We will show below that the results of our analysis depend little on specific details of the regulator.

4 Fits and results for the phase shifts

Having specified the regularization, we now describe the fit procedure and show our results for phase shifts. We begin with specifying the values of the LECs and masses that enter the potentials. Here and in what follows, we use $m_p = 938.272\,{\rm MeV}$, $m_n = 939.565\,{\rm MeV}$ for the nucleon masses and $M_{\pi^\pm} = 139.57\,{\rm MeV}$ and $M_{\pi^0} = 134.98\,{\rm MeV}$ for the charged and neutral pion masses, respectively. For the average pion mass which enters the expressions for the TPEP the value $M_\pi = 138.03\,{\rm MeV}$ is adopted. Further, we use the values $F_\pi = 92.4\,{\rm MeV}$ and $g_A = 1.267$ for the pion decay and nucleon axial coupling constants. Starting from NLO, one needs to account for the Goldberger-Treiman discrepancy which can be achieved via the replacement

$$g_A \to g_A - 2d_{18}M_\pi^2, \tag{28}$$

where d_{18} is a LEC from the sub-subleading pion-nucleon effective Lagrangian. Following [16], we adopt the larger value $g_A = 1.29$ instead of $g_A = 1.267$ in order to account for the Goldberger-Treiman discrepancy in the expressions for the OPEP and, at N^{3}LO, also for the leading TPEP. Using the Goldberger-Treiman relation $g_{\pi N} = g_A m_N/F_\pi$, this value of g_A leads to $g_{\pi N}^2/(4\pi) = 13.67$ which is consistent with the recent determination via the Goldberger-Miyazawa-Oehme sum rule [70], $g_{\pi N}^2/(4\pi) = 13.69 \pm 0.20$, as well as with the older determinations from NN [44] and πN [71] scattering data.

It remains to specify the πN LECs c_i and d_i which enter the TPEP at N^{3}LO. In table 1, we list the values of the c_i's adopted in the N^{3}LO potentials of refs. [16,17] and in the current work together with the empirical values determined from pion-nucleon scattering inside the Mandelstam triangle (fit 1). Using this unphysical kinematics in combination with dispersion relations has the advantage that the chiral expansion converges faster than in the physical region. Thus, one expects the determined LECs to have smaller theoretical uncertainties due to truncation of the chiral expansion as compared to fits in the physical region. For the LEC c_2, which could not be reliably determined in [72], we give the value from the order Q^3 heavy-baryon calculation of ref. [47]. We emphasize that several more recent determinations of these LECs from πN scattering up to order Q^4 in the heavy-baryon as well as manifestly covariant formulations of chiral perturbation theory

[5] Given that locally regularized potentials $V(\vec{q})$ show only a power-law decrease for high values of momentum transfer q, much higher virtual momenta are involved in solving the LS equation as compared to the nonlocal chiral potentials of refs. [16,17].

Table 1. Values of the LECs c_i in units of GeV^{-1} used in the various N^{3}LO NN potentials in comparison with the empirically determined values from πN scattering as described in the text.

LEC	N^{3}LO potential of ref. [17]	N^{3}LO potential of ref. [16]	This work	Empirical
c_1	-0.81	-0.81	-0.81	-0.81 ± 0.15 [72]
c_2	$2.80^{(a)}$	3.28	3.28	3.28 ± 0.23 [47]
c_3	$-3.20^{(a)}$	$-3.40^{(b)}$	-4.69	-4.69 ± 1.34 [72]
c_4	$5.40^{(a)}$	3.40	3.40	3.40 ± 0.04 [72]

(a) Fit parameter.
(b) Larger in magnitude values were found to lead to spurious deeply bound states.

are available, see, *e.g.*, [69, 73–76]. In addition, attempts were made to determine the LECs $c_{1,3,4}$ from nucleon-nucleon scattering data based on the two-pion exchange potential calculated at N^{2}LO [77–82] and N^{3}LO [17]. In particular, the values found in refs. [77, 79, 82] are consistent, within the quoted uncertainties, with the results obtained in pion-nucleon scattering. Notice, however, that none of these studies have addressed the question of the *systematic* theoretical uncertainties, in particular due to truncation of the chiral expansion for the potential at a given order. Accordingly, the interpretation of these findings is not completely clear. Very recently, ref. [83] has reported the determination of the LECs c_i from peripheral NN scattering using the N^{2}LO representation of the two-pion exchange potential. The c_4 value found in that work deviates significantly from its empirical value. Again, the systematic uncertainties associated with the adopted way of fitting only peripheral partial waves and with the truncation of the chiral expansion are not quantified in that analysis. Finally, for the LECs d_i from the order-Q^3 effective pion-nucleon Lagrangian which contribute to the N^{3}LO TPEP we adopt, following refs. [16, 17], the central values from fit 1 to πN phase shift given in ref. [47], namely

$$\begin{aligned} \bar{d}_1 + \bar{d}_2 &= 3.06\,\mathrm{GeV}^{-2}, \qquad \bar{d}_3 = -3.27\,\mathrm{GeV}^{-2}, \\ \bar{d}_5 &= 0.45\,\mathrm{GeV}^{-2}, \qquad \bar{d}_{14} - \bar{d}_{15} = -5.65\,\mathrm{GeV}^{-2}. \end{aligned} \tag{29}$$

For the regulator R, we employ the same range as used in the local versions of the N^{2}LO NN potential of ref. [61], namely $R = 0.8 \ldots 1.2\,\mathrm{fm}$. Specifically, we will carry out fits for five different values of R, namely $R = 0.8\,\mathrm{fm}$, $R = 0.9\,\mathrm{fm}$, $R = 1.0\,\mathrm{fm}$, $R = 1.1\,\mathrm{fm}$ and $R = 1.2\,\mathrm{fm}$. Notice that the smallest value of the cutoff R, $R = 0.8\,\mathrm{fm}$, coincides with the estimated distance at which the chiral expansion of the NN potential is expected to break down [66]. When transformed to momentum space using the relation $\Lambda = 2R^{-1}$ as motivated in the previous section, the employed cutoff range corresponds to the range of $\Lambda \simeq 500 \ldots 330\,\mathrm{MeV}$.

Following the procedure of the NPWA [45] which we use as input for our calculations, we fit all isospin-1 channels to pp phase shifts, which are accurately determined from the available scattering data, and generate np and nn phase shifts (with the exception of the $^1\mathrm{S}_0$ partial wave) by using the appropriate kinematical relations, see eqs. (A.2), (A.3) and (A.4), taking into account the isospin-breaking corrections to the OPEP due to the different pion masses, see eq. (3), and switching off the long-range electromagnetic interactions[6]. More precisely, pp phase shifts of ref. [45], which we use as input in our fits, actually correspond to phase shifts of the electromagnetic plus nuclear interaction with respect to electromagnetic wave functions, *i.e.* $\delta^{\mathrm{EM}}_{\mathrm{EM}+N}$ in the notation of ref. [45]. The dominant contributions to the long-range electromagnetic interaction are well known and include the usual static Coulomb potential, the leading relativistic correction to the Coulomb potential, the magnetic moment interaction and the vacuum polarization potential, see, *e.g.*, [16, 45] and references therein for more details and explicit expressions. Notice that the static Coulomb potential in combination with the leading relativistic correction is often referred to as the modified or relativistic Coulomb interaction. The NPWA employs the approximation $\delta^{\mathrm{EM}}_{\mathrm{EM}+N} \approx \delta^{\mathrm{C}}_{\mathrm{C}+N}$ for all pp channels except $^1\mathrm{S}_0$, where C means that the electromagnetic interaction is approximated by the Coulomb potential. For the $^1\mathrm{S}_0$ partial wave, the approximate relation between the phase shifts $\delta^{\mathrm{EM}}_{\mathrm{EM}+N}$ published in [45] and $\delta^{\mathrm{C}}_{\mathrm{C}+N}$ can be obtained using the distorted wave Born approximation. The resulting fairly model-independent shifts are tabulated in ref. [84] and appear to be negligibly small for energies larger than $E_{\mathrm{lab}} \sim 30\,\mathrm{MeV}$. Throughout this work, we use pp phase shifts corresponding to the modified Coulomb plus nuclear interaction with respect to the modified Coulomb wave functions and employ the corrections given in ref. [84] to relate these phase shifts to the ones of the NPWA [45] in the $^1\mathrm{S}_0$ partial wave. For the np case, the calculated and shown phase shifts are that of the nuclear interaction with respect to Riccati-Bessel functions. Notice that np phase shifts of the NPWA [45] actually correspond to $\delta^{\mathrm{MM}}_{\mathrm{MM}+N}$ since the electromagnetic interaction in that case

[6] Notice that such a "minimalistic" treatment of IB effects in the present analysis is dictated by using the NPWA results rather than NN experimental data as input for our fits. In particular, we do not take into account the known IB two-pion exchange contributions since they would induce shifts δ_{np}-δ_{pp} incompatible with the results of ref. [45]. A more complete treatment of IB corrections using NN experimental data is left for a future work.

is entirely given by the magnetic moment (MM) interaction within the NPWA. It is well known that the approximation [85] $\delta^{\rm EM}_{{\rm EM}+N} \approx \delta_N$ is rather accurate for all channels except for the ^{3}S$_1$ partial wave [85]. We will employ this standard approximation for *all* np partial waves in order to directly compare our phase shifts with the ones of the NPWA [45]. It should be understood that effects of the magnetic moment interaction in $\delta^{\rm MM}_{{\rm MM}+N}$ in the ^{3}S$_1$ channel of the NPWA [45] are mimicked by contact interactions in the potential when we calculate δ_N. We emphasize that our choice for the phase shifts throughout this work is the same as the one adopted, *e.g.*, in refs. [17,86].

For each value of the cutoff R, we determine the LECs accompanying the short-range operators specified in eq. (15) from a fit to np and pp phase shifts of the NPWA [45]. Specifically, we have in total 4 LECs at LO ($\tilde{C}_{3S1}$, $\tilde{C}^{\rm np}_{1S0}$, $\tilde{C}^{\rm pp}_{1S0}$ and $\tilde{C}^{\rm nn}_{1S0}$), 11 LECs at NLO and N^{2}LO ($\tilde{C}_{3S1}$, $\tilde{C}^{\rm np}_{1S0}$, $\tilde{C}^{\rm pp}_{1S0}$, $\tilde{C}^{\rm nn}_{1S0}$ and C_i) and 26 LECs at N^{3}LO ($\tilde{C}_{3S1}$, $\tilde{C}^{\rm np}_{1S0}$, $\tilde{C}^{\rm pp}_{1S0}$, $\tilde{C}^{\rm nn}_{1S0}$, C_i and D_i). Notice that while it is not necessary to account for isospin breaking at LO from the point of view of power counting, we decided to include the same isospin-breaking corrections in order to be consistent with the procedure of the NPWA and to allow for a meaningful comparison of results at different orders. The fits are carried out using the same energies as employed in the multi-energy partial wave analysis of the Nijmegen group, namely $E_{\rm lab}$ = 1, 5, 10, 25, 50, 100, 150 and 200 MeV[7]. Specifically, we use the energies $E_{\rm lab} \leq 25$ MeV at LO, $E_{\rm lab} \leq 100$ MeV at NLO and N^{2}LO and $E_{\rm lab} \leq 200$ MeV at N^{3}LO. The results for phase shifts at higher energies are thus to be regarded as predictions.

At N^{3}LO, we found that fits in the ^{3}S$_1$-^{3}D$_1$ become unstable, which manifests itself in the appearance of different solutions which describe equally well the ^{3}S$_1$ and ^{3}D$_1$ phase shifts and the mixing angle ϵ_1. This feature becomes especially disturbing for the hardest cutoff choices of $R = 0.8$ fm and $R = 0.9$ fm and indicates that 8 unknown LECs in this channel offer too much flexibility in the description of the phase shifts and the mixing angle. In addition to requiring that the resulting LECs are of natural size, we decided to impose further constraints to stabilize the fits in this channel. In particular, we demand that the deuteron binding energy is correctly reproduced and discard solutions which lead to unrealistic values of the D-state probability in the deuteron or show a too strong violation of the Wigner $SU(4)$ symmetry which implies the relation $\tilde{C}_{1S0} \simeq \tilde{C}_{3S1}$ [87], see also ref. [88]. It should be emphasized that the deuteron D-state probability P_D is not a measurable quantity and can be changed by means of a unitary transformation [89]. Modern phenomenological NN potentials typically yield the values of P_D in the range of $P_D = 4 \ldots 6\%$. In particular, the AV18 [85], Nijmegen I and II and Reid93 [90] potentials have $P_D = 5.76\%$, $P_D = 5.66\%$ $P_D = 5.64\%$ and $P_D = 5.70\%$, respectively, while the CD-Bonn potential [86] leads to a smaller value of $P_D = 4.85\%$, see ref. [91] for a related discussion. Furthermore, the chiral N^{3}LO potential of refs. [17] yields $P_D = 4.51\%$ while the ones of ref. [16] lead to even smaller values. It is conceivable that NN potentials corresponding to the choice of unitary transformation leading to values of P_D very different from the ones listed above would require strong many-body forces and exchange currents, the feature which is certainly worrisome in the context of effective field theory but also from the computational point of view, see, *e.g.*, the discussion in ref. [92]. Thus, we decided to introduce the deuteron D-state probability $P_D = 5\% \pm 1\%$ as an additional "data" point in the fit. As for the second constraint on the value of $\tilde{C}_{3S1}$, we employ a simple "augmented χ^2" following the lines of ref. [93] to penalize those values of $\tilde{C}_{3S1}$ which are considerably different from the ones of $\tilde{C}_{1S0}$ for the same choice of the cutoff. In practice, this is achieved by using

$$\chi^2_{\rm aug} = \chi^2 + \chi^2_{\rm prior}, \qquad \text{with} \qquad \chi^2_{\rm prior} = \frac{(\tilde{C}_{3S1} - \tilde{C}_{1S0})^2}{(\Delta\tilde{C}_{3S1})^2}\,, \tag{30}$$

where we choose $\Delta\tilde{C}_{3S1} = \tilde{C}_{1S0}/4$. Notice that this additional constraint is, in fact, only active for the two hardest choices of the cutoff as the unconstrained fits in other cases already lead to $\tilde{C}_{3S1} \simeq \tilde{C}_{1S0}$. For example, the value for $\tilde{C}_{3S1}$ resulting from the unconstrained fit with the cutoff $R = 1$ fm appears to lie within 1% of the value of $\tilde{C}_{1S0}$. We also found that different choices $\Delta\tilde{C}_{3S1} = \tilde{C}_{1S0}/2$, $\Delta\tilde{C}_{3S1} = \tilde{C}_{1S0}/3$, $\Delta\tilde{C}_{3S1} = \tilde{C}_{1S0}/5$ lead to negligibly small differences in the resulting observables.

Having specified the details of the fitting procedure, we are now in the position to discuss the results. In table 2, we give the obtained values of the various LECs at N^{3}LO for different choices of the cutoff R. It is important to keep in mind that the LECs correspond to bare quantities and are expected to depend significantly on the chiral order, employed regularization scheme and the choice of the cutoff. Although the LECs at NLO and N^{2}LO were demonstrated in ref. [88] to be well described in terms of resonance saturation by heavy-meson exchanges, it makes generally little sense to directly compare the LECs obtained by using different regularization schemes with each other. For example, due to the choice of a Gaussian regulator for contact interactions adopted in the present work, the LECs D_i contain contributions induced by contact interactions at lower orders driven by the LECs $\tilde{C}_i$ and C_i. A more meaningful comparison between the different approaches should rather be done at the level of observables or, more generally, renormalized quantities. What is, however, important to verify is that the obtained LECs are of a natural size. The natural size for the various LECs can be roughly estimated as [16]

$$|\tilde{C}_i| \sim \frac{4\pi}{F_\pi^2}, \qquad |C_i| \sim \frac{4\pi}{F_\pi^2 \Lambda_b^2}, \qquad |D_i| \sim \frac{4\pi}{F_\pi^2 \Lambda_b^4}\,, \tag{31}$$

where the factor of 4π emerges from the angular integration in the partial wave decomposition and Λ_b is the pertinent hard scale. If the scale Λ_b is identified with the

[7] We will also include the energies of 250 and 300 MeV when discussing the quality of the fits below.

Table 2. The LECs $\tilde{C}^{\rm pp}_{1S0}$, $\tilde{C}^{\rm nn}_{1S0}$, $\tilde{C}^{\rm np}_{1S0}$, $\tilde{C}_{3S1}$, C_i and D_i at N^{3}LO for different values of the cutoff R. The values of the $\tilde{C}_i$, C_i and D_i are given in units of $10^4\,\mathrm{GeV}^{-2}$, $10^4\,\mathrm{GeV}^{-4}$ and $10^4\,\mathrm{GeV}^{-6}$, respectively.

LEC	$R=0.8\,\mathrm{fm}$	$R=0.9\,\mathrm{fm}$	$R=1.0\,\mathrm{fm}$	$R=1.1\,\mathrm{fm}$	$R=1.2\,\mathrm{fm}$
$\tilde{C}^{\rm pp}_{1S0}$	0.2363	0.1648	0.1090	0.0574	0.0166
$\tilde{C}^{\rm nn}_{1S0}$	0.2352	0.1631	0.1070	0.0551	0.0140
$\tilde{C}^{\rm np}_{1S0}$	0.2328	0.1600	0.1035	0.0513	0.0100
C_{1S0}	−0.0433	−0.0400	−0.1155	−0.2078	−0.3344
D^1_{1S0}	3.0691	−1.8080	−6.9812	−13.3659	−21.9934
D^2_{1S0}	0.6135	3.0136	6.4537	10.8060	16.5111
C_{3P0}	1.0678	0.7812	0.5120	0.2645	0.0313
D_{3P0}	−0.4030	0.6311	1.5809	2.5084	3.4432
C_{1P1}	1.0068	0.8095	0.6926	0.6267	0.5930
D_{1P1}	0.9480	1.6652	2.4623	3.4613	4.7819
C_{3P1}	1.3413	1.1253	0.9667	0.8592	0.7865
D_{3P1}	−0.7070	0.3656	1.4145	2.6058	4.1340
$\tilde{C}_{3S1}$	0.2441	0.1688	0.1043	0.0513	0.0097
C_{3S1}	−0.3292	−0.3844	−0.4256	−0.4868	−0.5790
D^1_{3S1}	−4.5205	−8.0894	−12.3514	−17.5859	−23.6921
D^2_{3S1}	3.8438	6.4034	9.2050	12.3977	15.7636
$C_{3D1\text{-}3S1}$	0.3424	0.4092	0.5388	0.7298	0.9624
$D^1_{3D1\text{-}3S1}$	0.8641	−0.3181	−2.0898	−4.3925	−7.3943
$D^2_{3D1\text{-}3S1}$	−1.5054	−0.3157	1.6466	4.2798	8.0089
D_{3D1}	1.4422	1.2225	1.1240	1.1446	1.1740
D_{1D2}	1.3770	0.9617	0.4782	−0.1144	−0.8569
D_{3D2}	0.6540	0.0259	−0.8805	−2.1386	−3.8116
C_{3P2}	0.5639	0.3189	0.1418	0.0134	−0.0768
D_{3P2}	−0.5008	−0.4398	−0.6095	−1.0773	−1.9421
$D_{3F2\text{-}3P2}$	−0.1355	−0.2343	−0.4108	−0.6946	−1.1275
D_{3D3}	−0.1655	−0.4103	−0.7289	−1.1377	−1.6564

employed ultraviolet cutoff $\Lambda = 2R^{-1}$, the expected natural size of the LECs $|\tilde{C}_i|$, $|C_i|$ and $|D_i|$ is $0.15\times10^4\,\mathrm{GeV}^{-2}$, $0.6\times10^4\,\mathrm{GeV}^{-4}$ ($1.4\times10^4\,\mathrm{GeV}^{-4}$) and $2.5\times10^4\,\mathrm{GeV}^{-6}$ ($13\times10^4\,\mathrm{GeV}^{-6}$), respectively, for the hardest (softest) employed cutoff $R=0.8\,\mathrm{fm}$ ($R=1.2\,\mathrm{fm}$). This would imply that all obtained LECs are of a natural size. On the other hand, as we will show in the next section, the actual breakdown scale Λ_b in our case appears to be somewhat larger than the UV cutoff $\Lambda = 2R^{-1}$. In particular, we will use $\Lambda_b = 400\ldots600\,\mathrm{MeV}$, depending on the employed value of R, for estimating the theoretical uncertainty in sect. 7. This implies that the natural size of the LECs $|C_i|$ and $|D_i|$ is expected to be $0.4\times10^4\,\mathrm{GeV}^{-4}$ ($0.9\times10^4\,\mathrm{GeV}^{-4}$) and $1.1\times10^4\,\mathrm{GeV}^{-6}$ ($6\times10^4\,\mathrm{GeV}^{-6}$), respectively, for the hardest (softest) cutoff choices. Also for such an estimation, all LECs are of a natural size (with the values of D^1_{3S1} appearing to be somewhat large in magnitude).

In fig. 3, we show our results at different orders in the chiral expansion for np phase shifts and mixing angles used in the N^{3}LO fit. Here, we restrict ourselves to one particular cutoff choice, namely $R=0.9\,\mathrm{fm}$, in order to have not too many lines in the plots. The cutoff dependence of our results will be addressed in sects. 5 and 7. One clearly observes a good convergence pattern with the N^{3}LO results being in excellent agreement with the NPWA in the whole considered range of energies. The convergence pattern is in most cases qualitatively similar to the one reported in ref. [16] although there are differences in certain channels. For example, for the ^{3}P$_0$ partial wave, the results at NLO and N^{2}LO of ref. [16] indicate too much repulsion at higher energies while the opposite is observed in our analysis. Still, these results are consistent with each other within the estimated theoretical uncertainty at these orders, see sect. 7 for more details. Concerning the N^{3}LO results, the improved NN potential of this work shows a superior performance in the whole considered energy range compared to the potential of ref. [16] as will be shown below. We attribute this feature primarily to a better choice of regularization, see sect. 3 for more details. We also emphasize that our N^{3}LO results for peripheral, *i.e.* F- and higher partial waves not shown in fig. 3 are similar to the ones reported in refs. [16, 95]. In particular, we also observe large relative deviations for F-waves at higher energies. For example, for the cutoff $R=0.9\,\mathrm{fm}$, we find $\delta^{\rm np}_{3F2} = 3.1^\circ$ at $E_{\rm lab} = 250\,\mathrm{MeV}$ to be compared with the NPWA result $\delta^{\rm np}_{3F2} = 1.4^\circ$. Notice, however, that *absolute* deviations from the NPWA for F-waves appear to be of

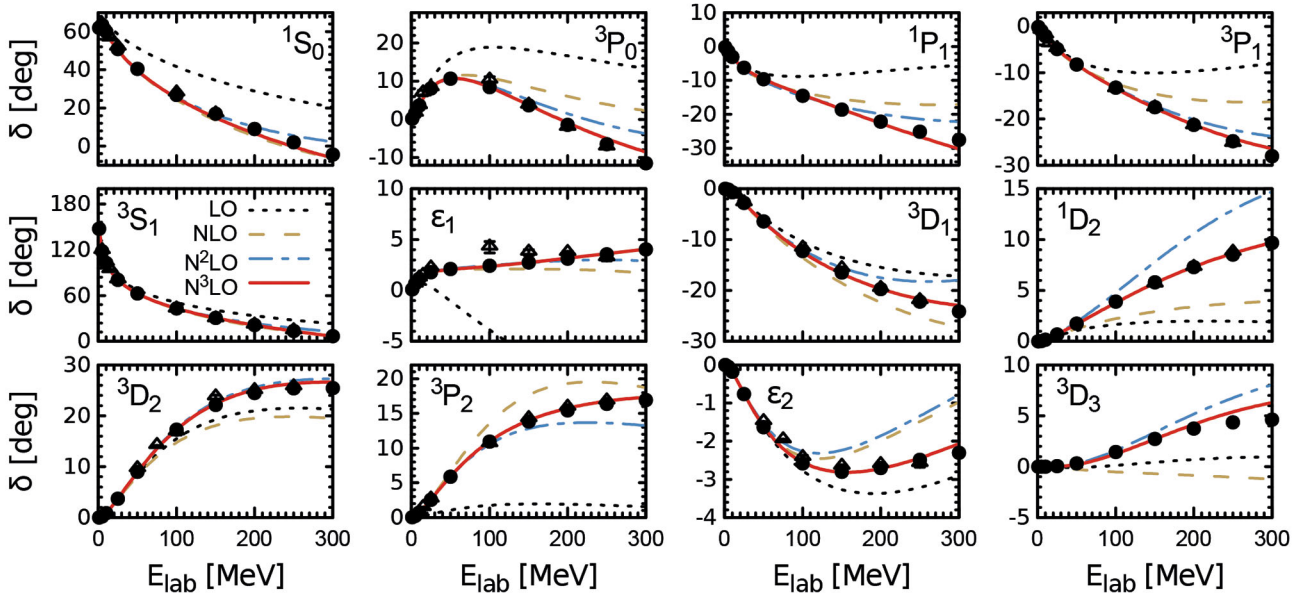

Fig. 3. (Color online) Chiral expansion of the NN phase shifts in comparison with the NPWA [45] (solid dots) and the GWU single-energy np partial wave analysis [94] (open triangles). Dotted, dashed (brown), dash-dotted (blue) and solid (red) lines show the results at LO, NLO, N^{2}LO and N^{3}LO, respectively, calculated using the cutoff $R = 0.9$ fm. Only those partial waves are shown which have been used in the fits at N^{3}LO.

a similar size as the ones observed in low partial wave so that there is no reason to expect the theoretical uncertainty in low-energy observables to be dominated by the discrepancies in F-waves. It is conceivable that the deviations for F-waves will be largely reduced by the order-Q^6 contact interactions.

It is desirable to have a quantitative criterium for comparing the accuracy of different potentials with each other. Usually, this is achieved by calculating the χ^2/datum for the reproduction of the available np and pp scattering data. Presently, we do not have the necessary machinery to carry out such a calculation and reserve this task for a future study. In the present work, we employ a simpler approach and calculate $\tilde{\chi}^2$/datum for the reproduction of the *phase shifts* of the NPWA used as input in our analysis. Here and in what follows, we will use a symbol $\tilde{\chi}^2$ for such an approach in order to avoid a possible confusion with χ^2 for the description of experimental data. Specifically, we calculate $\tilde{\chi}^2$/datum at energies of $E_{\rm lab} = 1$, 5, 10, 25, 50, 100, 150, 200, 250 and 300 MeV employed in the NPWA and also in our fits. Unfortunately, the NPWA [45] only provide statistical errors which do not include systematic uncertainties. In order to have a meaningful definition of $\tilde{\chi}^2$, we define the uncertainty for a given phase shift (or mixing angle) δ in the channel X at a given energy as

$$\Delta_X = \max\Big(\Delta_X^{\rm NPWA},\ \Big|\delta_X^{\rm NijmI} - \delta_X^{\rm NPWA}\Big|,\ \Big|\delta_X^{\rm NijmII} - \delta_X^{\rm NPWA}\Big|,\ \Big|\delta_X^{\rm Reid93} - \delta_X^{\rm NPWA}\Big|\Big), \qquad (32)$$

where $\delta_X^{\rm NPWA}$ and $\Delta_X^{\rm NPWA}$ refer to the phase shift (or mixing angle) in the channel X and the corresponding statistical error of the NPWA, respectively, while $\delta_X^{\rm NijmI}$, $\delta_X^{\rm NijmI}$ and $\delta_X^{\rm Reid93}$ denote the results based on the Nijmegen I, II and Reid93 NN potentials of ref. [90]. These phenomenological potentials are constructed using the same database as employed in the NPWA and have a nearly optimal χ^2/datum of 1.03. For this reason, they have, in fact, been suggested as alternative partial wave analyses [90]. While the above definition of uncertainties provides a reasonable estimation, one should not overinterpret the resulting values for $\tilde{\chi}^2$/datum calculated based on the NPWA phase shifts in the way specified above[8]. In particular, there is no statistical interpretation of the value of $\tilde{\chi}^2$/datum. We, nevertheless, still find this approach useful for the sake of a simple comparative analysis of the accuracy of different NN potentials. We also used the errors defined above in all our fits.

In table 3 we show the $\tilde{\chi}^2$/datum for the description of the Nijmegen np and pp phase shifts in those channels which were used in the fit at N^{3}LO, namely S-, P, and D-waves and the mixing angles ϵ_1 and ϵ_2. As a test of our approach, we first apply it to the CD-Bonn potential of ref. [86]. The resulting values for $\tilde{\chi}^2$/datum clearly indicate that this potential provides a very good description of both the np and pp phase shifts of the NPWA in the whole energy range. Notice that the CD-Bonn potential was fitted to a considerably larger database as compared to the NPWA. For the Idaho N^{3}LO potentials of ref. [17], the $\tilde{\chi}^2$/datum appears to be somewhat higher, especially for the version with the cutoff $\Lambda = 600$ MeV. Notice that

[8] There is no obvious relation between $\tilde{\chi}^2$/datum for the description of NPWA phase shifts and that for the description of real data. In particular, our simplistic approach does not take into account the fact that peripheral partial waves are less important for the description of low-energy observables.

Table 3. $\tilde{\chi}^2$/datum for the description of the Nijmegen np and pp phase shifts [45] as described in the text. Only those channels are included which have been used in the N^{3}LO fits, namely the S-, P- and D-waves and the mixing angles ϵ_1 and ϵ_2.

$E_{\rm lab}$ bin	CD-Bonn	Idaho N^{3}LO		N^{3}LO of [16]	Improved chiral potentials at N^{3}LO, this work				
(MeV)		(500)	(600)	(550/600)	$R = 0.8$ fm	$R = 0.9$ fm	$R = 1.0$ fm	$R = 1.1$ fm	$R = 1.2$ fm
Neutron-proton phase shifts									
0–100	0.6	1.7	5.2	1.9	0.8	0.7	0.6	0.7	1.4
0–200	0.6	2.2	5.3	2.1	0.8	0.7	0.6	0.8	1.8
0–300	0.6	3.3	6.8	6.0	2.1	1.5	1.8	4.0	10.7
Proton-proton phase shifts									
0–100	0.5	1.5[(a)]	6.7[(a)]	8.3	1.8	0.8	0.5	1.2	4.6
0–200	1.3	2.9[(a)]	11.7[(a)]	14.7	2.1	0.7	0.6	2.2	8.2
0–300	1.3	5.9[(a)]	30.0[(a)]	75.3	12.0	3.2	7.0	24.5	66.8

[(a)] The $^1S_0$ partial wave has not been taken into account as explained in the text.

we did not include the pp ^{1}S$_0$ phase shift when calculated the $\tilde{\chi}^2$/datum for the Idaho N^{3}LO potentials. This is because the authors of ref. [17] employed a more elaborated treatment of IB corrections as compared to the NPWA. This is especially important for the splitting between the pp and np ^{1}S$_0$ phase shifts and would result in a very large $\tilde{\chi}^2$/datum if the pp ^{1}S$_0$ phase would be included. It is interesting to compare these findings with χ^2/datum for the reproduction of the real data. The values quoted in ref. [86] for the CD-Bonn potential, namely χ^2/datum = 1.02 for np and χ^2/datum = 1.01 for pp data below 350 MeV and in ref. [17] for the two versions of the Idaho potentials, namely χ^2/datum = 1.1–1.3 for np and χ^2/datum = 1.5–2.1 for pp data below 290 MeV, show clearly the same qualitative trend. On the other hand, it is clear that $\tilde{\chi}^2$/datum employed in our analysis is a much more sensitive quantity and the values of $\tilde{\chi}^2$/datum ~ 5 do still correspond to accurate description of real data. In particular, deviations from the NPWA for D-waves or the mixing angle ϵ_2 are reflected in the calculated value of $\tilde{\chi}^2$/datum while their effect on scattering observables at low energy is suppressed due to their threshold behavior.

The results for $\tilde{\chi}^2$/datum for the improved chiral potential of the present work at different values of the cutoff R are listed in the last five columns of table 3. Given that the softest cutoff $R = 1.2$ fm corresponds to the momentum-space regulator of $\Lambda \sim 330$ MeV, the large values of $\tilde{\chi}^2$/datum for this cutoff in the whole energy range of $E_{\rm lab} = 0$–300 MeV simply reflect the feature that the potential is used at energies beyond its applicability range. The same applies, to a lesser extent, to the cutoff $R = 1.1$ fm which corresponds to the momentum-space cutoff of $\Lambda \sim 360$ MeV. As expected, decreasing the value of the coordinate-space cutoff R leads to a better description of the phase shifts. The improvement stops for the hardest considered cutoff of $R = 0.8$ fm. Notice that the corresponding momentum cutoff $\Lambda \sim 500$ MeV is considerably larger than the one found in ref. [23], where the TPEP was neglected. Our findings thus confirm the importance of the two-pion exchange, see also refs. [77, 96] for a related discussion. Altogether, the description of the np and pp phase shifts based on the improved N^{3}LO interactions is excellent for energies below 200 MeV and, for the optimal cutoff choice of $R = 0.9$ fm, even up to $E_{\rm lab} = 300$ MeV.

Table 4. $\tilde{\chi}^2$/datum for the description of the Nijmegen np and pp phase shifts [45] as described in the text at different orders in the chiral expansion for the cutoff $R = 0.9$ fm. Only those channels are included which have been used in the N^{3}LO fits, namely the S-, P- and D-waves and the mixing angles ϵ_1 and ϵ_2.

$E_{\rm lab}$ bin	LO	NLO	N^{2}LO	N^{3}LO
Neutron-proton phase shifts				
0–100	360	31	4.5	0.7
0–200	480	63	21	0.7
Proton-proton phase shifts				
0–100	5750	102	15	0.8
0–200	9150	560	130	0.7

It is also interesting to compare the reproduction of the Nijmegen phase shifts at different orders in the chiral expansion. In table 4 we show the corresponding values of $\tilde{\chi}^2$/datum for the cutoff $R = 0.9$ fm. The observed pattern provides yet another indication that the chiral expansion for the nuclear force converges well, see also fig. 3. It is especially comforting to see the improvement when going from NLO to N^{2}LO which is entirely due to the subleading TPEP. Notice that the number of adjustable parameters is the same at NLO and N^{2}LO. Last but not least, our results seem to support the validity of Weinberg's power counting and do not indicate the need for its modification as suggested, *e.g.*, in refs. [25–27].

5 Cutoff dependence

We now address in some detail the residual cutoff dependence of our results. As explained at the beginning of sect. 3, the dependence of observables on the cutoff R

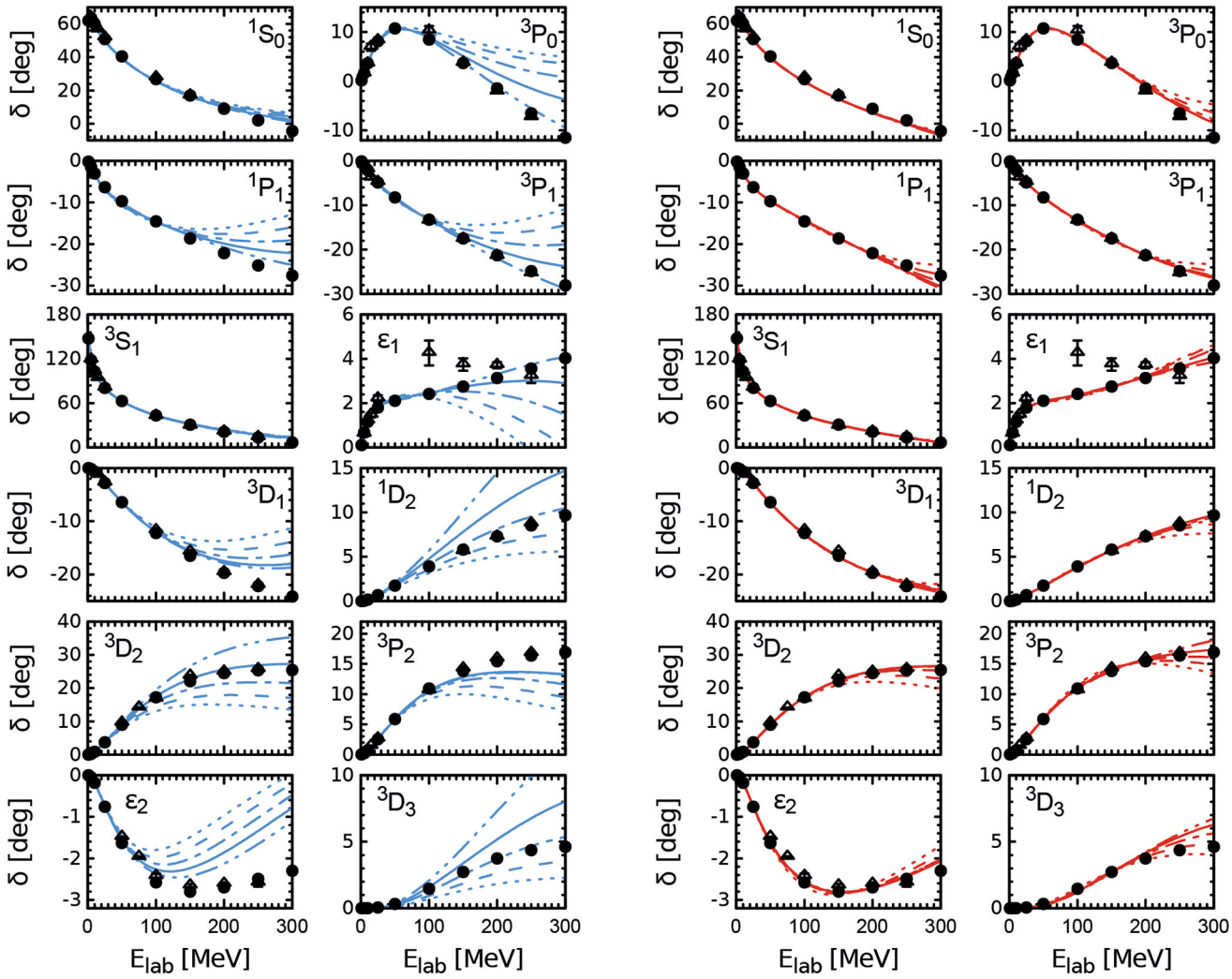

Fig. 4. Cutoff dependence of the phase shifts calculated at N^{2}LO (left panel) and N^{3}LO (right panel). Dotted, dashed, dash-dotted, solid and dash-double-dotted lines show the results obtained with the cutoffs $R = 1.2\,\mathrm{fm}$, $R = 1.1\,\mathrm{fm}$, $R = 1.0\,\mathrm{fm}$, $R = 0.9\,\mathrm{fm}$ and $R = 0.8\,\mathrm{fm}$, respectively. Only those partial waves are shown which have been used in the fits at N^{3}LO. Solid dots and open triangles correspond to the results of the NPWA [45] and the GWU single-energy np partial wave analysis [94].

is *not* completely removed in our calculations, see however ref. [31] for an alternative renormalizable approach. The residual cutoff dependence can be viewed as an estimation of effects of higher-order contact interactions beyond the truncation level of the potential, see, however, the discussion in sect. 7. One, therefore, expects the residual cutoff dependence to reduce when going from LO to NLO/N^{2}LO and from NLO/N^{2}LO to N^{3}LO/N^{4}LO. On the other hand, the residual cutoff dependence at chiral orders NLO and N^{2}LO as well as N^{3}LO and N^{4}LO is expected to be of the same size. In fig. 4 we compare the cutoff dependence of the S-, P- and D-wave phase shifts and the mixing angles ϵ_1 and ϵ_2 at N^{2}LO and N^{3}LO. The cutoff dependence at N^{3}LO appears to be very weak in all channels used in the fit. In particular, it is considerably weaker than the one resulting from our N^{3}LO potential [16] where a nonlocal exponential regulator was employed for the OPEP, TPEP and the contact interactions. The new regularization scheme described in sect. 3 shows a superior performance at higher energies and produces only a small amount of artefacts (*i.e.* the residual cutoff dependence) in the considered energy range.

To get more insights into the residual cutoff dependence of phase shift δ in a given channel, we follow the lines of ref. [97, 98] and plot in fig. 5 the quantity $|1-\cot\delta_{R_1}(k)/\cot\delta_{R_2}(k)|$, where R_1 and R_2 are two different values of the cutoff, as function of the cms momentum k. Specifically, we choose $R_1 = 0.9\,\mathrm{fm}$ and $R_2 = 1.0\,\mathrm{fm}$ and restrict ourselves to the np ^{1}S$_0$, ^{3}S$_1$, ^{3}P$_1$ and ^{3}P$_2$ partial waves which may serve as representative examples. First, the resulting error plots demonstrate a very similar cutoff dependence at NLO and N^{2}LO which is to be expected based on general arguments as discussed above. In addition, one observes that the cutoff dependence reduces significantly in the whole range of momenta when going from LO to NLO/N^{2}LO and from NLO/N^{2}LO to N^{3}LO/N^{4}LO.

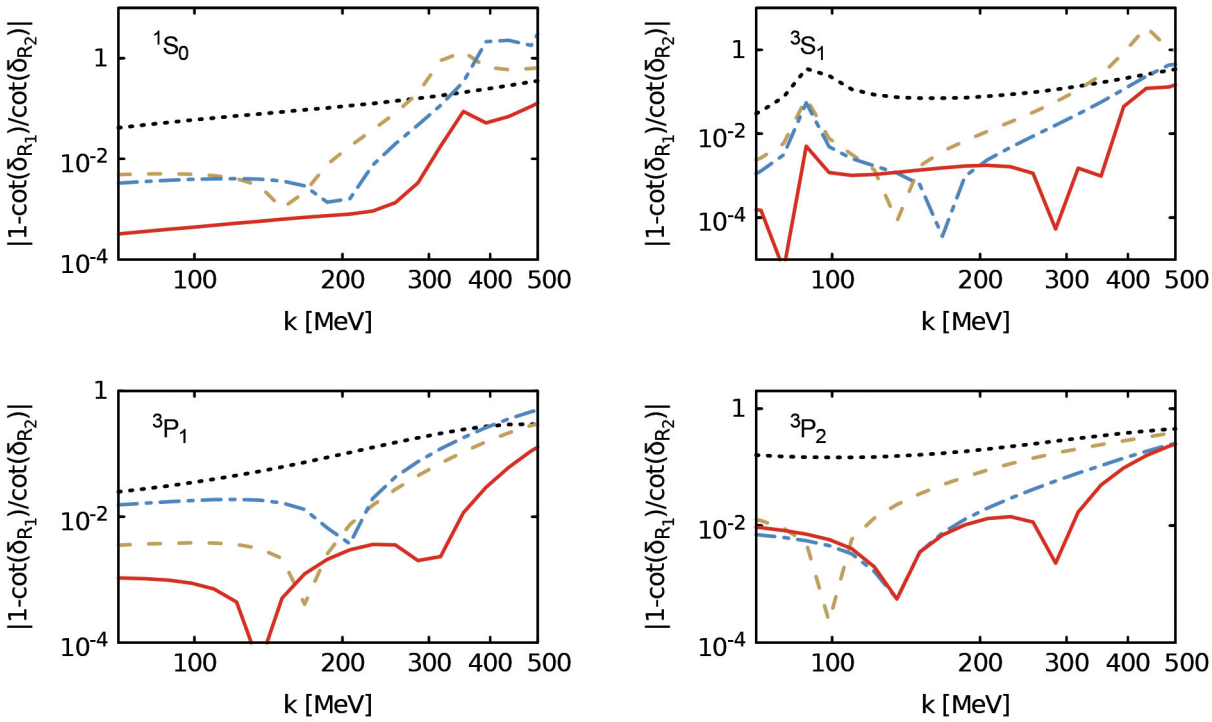

Fig. 5. (Color online) Error plots for np scattering in the $^1S_0$, $^3S_1$, $^3P_1$ and $^3P_2$ partial waves as explained in the text. Dotted, dashed (brown), dash-dotted (blue) and solid (red) lines show the results at LO, NLO, N^{2}LO and N^{3}LO, respectively.

Notice that the appearance of dips in the plots at values of k where the function $1-\cot\delta_{R_1}(k)/\cot\delta_{R_2}(k)$ changes its sign has no significance and should be ignored. Also, the structures seen in the $^3S_1$ partial wave for $k\sim 90\,\mathrm{MeV}$ and $k\sim 400\,\mathrm{MeV}$ ($^1S_0$ partial wave for $k\sim 350\ldots 400\,\mathrm{MeV}$) simply reflect the feature that $\cot(\pi/2)=0$ ($\cot(0)=\infty$) and should be ignored, too. Concerning the slope of the curves at different orders, the error plots indicate the appearance of two different regimes: at low momenta well below the pion mass, the slope does not change significantly from order to order and the curves are nearly horizontal. This is a qualitatively similar pattern to the one reported in ref. [97]. To understand this feature, we recall that chiral expansion of the nuclear force is actually a double expansion in powers of momenta and the pion mass M_π, see eq. (1). At low momenta, we expect the corrections to be dominated by powers of M_π/Λ_b and, therefore, to be nearly independent on momenta. On the other hand, at momenta above the pion mass, one may expect the corrections to be dominated by powers of k/Λ_b. The increase of the slope when going from LO to NLO/N^{2}LO and from NLO/N^{2}LO to N^{3}LO can be viewed as a self-consistency check of the calculation and indicates that the theory is properly renormalized, see refs. [23, 99] for more details. Finally, we read off from the plots that the breakdown scale Λ_b at N^{3}LO, *i.e.* the momenta at which the N^{3}LO curves cross the ones of lower orders, is about $\sim 500\,\mathrm{MeV}$ for S-waves and even higher for P-waves. These observations are in line with our previous findings and, in particular, with the size of the LECs accompanying the corresponding contact interactions which are listed in table 2. We will use $\Lambda_b = 400\ldots 600\,\mathrm{MeV}$, depending on the cutoff R, in our estimation of the theoretical uncertainties in sect. 7. It would be interesting to see whether and how the explicit inclusion of the $\Delta(1232)$ degrees of freedom in the effective Lagrangian will affects the breakdown scale of the EFT expansion.

6 Deuteron properties

We now turn to the deuteron properties. First, as already emphasized in sect. 4, we stress that we used the binding energy $B_d = 2.224575\,\mathrm{MeV}$ [100] to constrain the fit. While this choice differs from our early work [16], it is actually the standard procedure for all high-precision phenomenological potentials such as the Nijmegen I, II, Reid93, CD-Bonn and AV18 one. Also the N^{3}LO potential of ref. [17] was tuned to reproduce the experimental value of the deuteron binding energy. We anticipate that relaxing this condition in the fits would have little impact on few-nucleon observables.

In table 5, we collect various deuteron properties at N^{3}LO using different values of the cutoff R in comparison with the results based on the CD-Bonn [86], N^{3}LO Idaho (500) [17] and N^{3}LO (550/600) [16] potentials and with empirical numbers. In all cases with the exception of the N^{3}LO Idaho potential, the deuteron binding energy is calculated based on relativistic kinematics, see eq. (A.4) and refs. [16, 86] for more details. We remind the reader that the asymptotic S state normalization A_S and the asymptotic D/S state ratio η are observable quantities which

Table 5. Deuteron binding energy B_d, asymptotic S state normalization A_S, asymptotic D/S state ratio η, radius r_d and quadrupole moment Q predicted by various NN potential in comparison with empirical information. Also shown is the D-state probability P_D. Notice that r_d and Q_d are calculated without taking into account meson-exchange current contributions and relativistic corrections.

	CD-Bonn, [86]	Idaho N^{3}LO (500), [17]	N^{3}LO of [16] (550/600)	Improved chiral potentials at N^{3}LO, this work					Empirical
				$R = 0.8$ fm	$R = 0.9$ fm	$R = 1.0$ fm	$R = 1.1$ fm	$R = 1.2$ fm	
B_d (MeV)	2.2246[(a)]	2.2246[(a)]	2.2196	2.2246[(a)]	2.2246[(a)]	2.2246[(a)]	2.2246[(a)]	2.2246[(a)]	2.224575(9)
A_S (fm$^{-1/2}$)	0.8846	0.8843	0.8820	0.8843	0.8845	0.8845	0.8846	0.8846	0.8846(9)
η	0.0256	0.0256	0.0254	0.0255	0.0255	0.0256	0.0256	0.0256	0.0256(4)
r_d (fm)	1.966	1.975	1.977	1.970	1.972	1.975	1.979	1.982	1.97535(85)
Q (fm^2)	0.270	0.275	0.266	0.268	0.271	0.275	0.279	0.283	0.2859(3)
P_D (%)	4.85	4.51	3.28	3.78	4.19	4.77	5.21	5.58	

[(a)] The deuteron binding energy has been taken as input in the fit.

can be extracted from the S-matrix at the deuteron pole by means of analytic continuation, see [16] and references therein. The empirical values for these quantities quoted in table 5 are taken from refs. [101,102]. For the deuteron radius r_d, the quoted value corresponds to the so-called deuteron structure radius which is defined as a square root of the difference of the deuteron, proton and neutron mean square charge radii and is taken from ref. [103]. It agrees well with the earlier result of $r_d = 1.971(5)$ fm reported in ref. [104]. For the quadrupole moment Q, the experimental value given in table 5 is from ref. [105].

Our predictions for A_S, η and r_d are in excellent agreement with the empirical numbers. Notice that our calculation of r_d and Q does not take into account relativistic and exchange current contributions. For the radius r_d, the corresponding corrections to r_d^2 were estimated in ref. [106] to give $0.014\,\mathrm{fm}^2$ while other calculations quote even smaller numbers. Thus, neglecting these contributions would affect the results for r_d at most at the level of 0.2% which is below the residual cutoff variation $\sim 0.6\%$ for this quantity at N^{3}LO.

For the quadrupole moment, our predictions underestimate the experimental value similarly to what is observed for other modern phenomenological potentials as well as for the chiral N^{3}LO potentials of refs. [16,17]. Notice that the amount of underestimation is largest for the hardest cutoff $R = 0.8$ fm and reduces strongly for the softest cutoff $R = 1.2$ fm. We also emphasize that relativistic and meson exchange current corrections, which are not included in our predictions, were estimated to increase the value of Q by the amount of $0.010\,\mathrm{fm}^2$ [86] based on the Bonn one-boson exchange model. This would bring our predictions for the quadrupole moment in agreement with the experimental value. This conclusion is also fully in line with the results of ref. [107], where the contributions from the relativistic corrections and one-pion exchange two-body charge operator were estimated to be $\Delta Q \simeq 0.008\,\mathrm{fm}^2$, see also ref. [108] for a related recent work. Adding this correction to our prediction yields $Q = 0.278 \ldots 0.291\,\mathrm{fm}^2$ in agreement with experiment. The residual cutoff dependence of Q is to be removed by the leading short-range two-body current. Its required contribution of the order of $\sim 2 \ldots 3\%$ is in agreement with the expected natural size of the corresponding LEC [107].

Table 6. Deuteron properties at various orders in the chiral expansion for the cutoff $R = 0.9$ fm in comparison with empirical values. For notation see table 5.

	LO	NLO	N^{2}LO	N^{3}LO	Empirical
B_d (MeV)	2.0235	2.1987	2.2311	2.2246[(a)]	2.224575(9)
A_S (fm$^{-1/2}$)	0.8333	0.8772	0.8865	0.8845	0.8846(9)
η	0.0212	0.0256	0.0256	0.0255	0.0256(4)
r_d (fm)	1.990	1.968	1.966	1.972	1.97535(85)
Q (fm^2)	0.230	0.273	0.270	0.271	0.2859(3)
P_D (%)	2.54	4.73	4.50	4.19	

[(a)] The deuteron binding energy has been taken as input in the fit.

It is also instructive to address convergence of the chiral expansion for the deuteron properties by looking at the predictions at different orders which are listed in table 6. Here we restrict ourselves to a single cutoff choice, namely $R = 0.9$ fm. One observes a good convergence of the chiral expansion for all listed quantities with the exception of P_D which is well known to be not observable.

Finally, we display in fig. 6 the deuteron wave functions calculated using the N^{3}LO potential of the present work in comparison with those based on the CD-Bonn and the N^{3}LO potentials of refs. [16, 17]. As a consequence of the employed regulator, the wave functions based on the improved chiral potentials are free from the oscillatory distortions observed in the case of the N^{3}LO potentials of refs. [16, 17] and are in a very good agreement with each other and with the wave functions of the CD-Bonn potential at distances larger than $r \sim 2 \ldots 3$ fm. Notice that momentum-space deuteron wave functions of the N^{3}LO potentials of refs. [16, 17] show significant deviations from the wave functions based on the phenomenological potentials at $p \sim 400$ MeV. These deviations were found in ref. [109] to be responsible for strong distortions in the predicted shape of the neutron-deuteron differential cross section around the minimum at the energy of

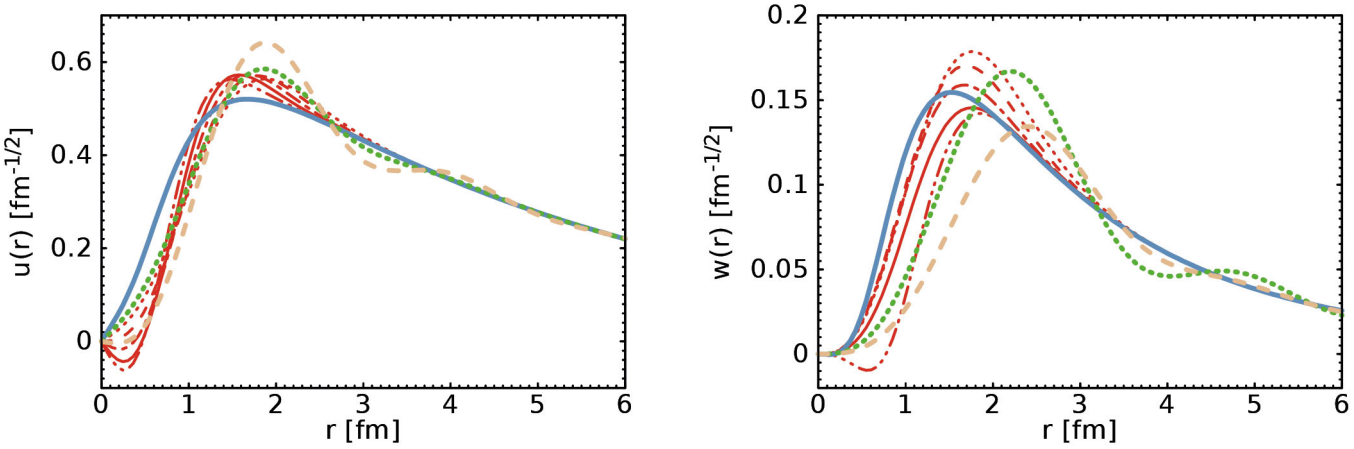

Fig. 6. Deuteron wave functions in coordinate space. Thin (red) dotted, dashed, dash-dotted, solid and dash-double-dotted lines show the results obtained using the N^{3}LO potentials of this work with the cutoffs $R = 1.2\,\text{fm}$, $R = 1.1\,\text{fm}$, $R = 1.0\,\text{fm}$, $R = 0.9\,\text{fm}$ and $R = 0.8\,\text{fm}$, respectively. Thick (green) dotted (light brown), dashed (blue) and solid lines refer to the wave functions of the Idaho (500) N^{3}LO potential of ref. [17], the N^{3}LO (550/600) potential of ref. [16] and the CD-Bonn potential [86].

$E_{\text{N,lab}} = 200\,\text{MeV}$. It would be interesting to investigate whether this problem still persists for the improved chiral potentials. Work along these lines is in progress.

7 Estimation of the theoretical uncertainty

We now turn to the discussion of uncertainty quantification in nuclear chiral EFT calculations, see ref. [99] for a recent paper on this topic. Here and in what follows, our considerations are restricted to few-nucleon systems, for which the quantum mechanical A-body problem is assumed to be (numerically) exactly solvable. This certainly applies at least to systems with $A \leq 4$. We will, therefore, not address uncertainties associated with methods for calculating observables.

There are various sources of uncertainties in nuclear Hamiltonian derived in the framework of chiral EFT which include, see also ref. [99]:

1) *Systematic* uncertainty due to truncation of the chiral expansion at a given order.
2) Uncertainty in the knowledge of πN LECs which govern the long-range part of the nuclear force.
3) Uncertainty in the determination of LECs accompanying contact interactions.
4) Uncertainties in the experimental data or, in our case, the NPWA used to determine the LECs.

In addition, results of the calculations are expected to show some sensitivity on the employed regularization framework. This issue will be addressed at the end of this section. Here and in what follows, we will primarily concentrate on the first item which, at the curent level of calculations, we believe to be the dominant source of uncertainty. We anticipate, based on the results reported in refs. [77–79, 81, 82], that the impact of the uncertainties in πN LECs and, especially in the order-Q^2 ones, *i.e.* the c_i, on the calculated NN observables might be significant. This issue should be investigated in a careful and systematic way in the future. A particularly promising approach to determine the values of the πN LECs would be to perform a simultaneous investigation of πN scattering and the reaction $\pi N \to \pi\pi N$, see refs. [110, 111] on the chiral EFT treatment of this process. Such an analysis goes beyond the scope of this work and is reserved for a future investigation.

The uncertainty in the determination of NN contact interaction is clearly affected by the employed fit procedure such as, in particular, the choice of energy range and weights adopted in the calculation of $\tilde{\chi}^2$. Following our early work of [16], we used fixed ranges in energies to tune the contact interactions as described in sect. 4 and checked in each case the stability of our results with respect to their variations. We did not employ additional weights in the $\tilde{\chi}^2$ to account for the expected increase of the theoretical uncertainty at higher energies, see ref. [83] for a different approach. Both of these issues can, in principle, be addressed in a systematic way within a Bayesian framework [93, 99]. This topic is postponed for a future study. Finally, *statistical* uncertainties for the LECs accompanying NN contact interactions at N^{2}LO were studied in ref. [81]. Their impact on selected pp and np phase shifts can be found in table 5 of that work and appears to be negligibly small compared to the *systematic* theoretical uncertainty to be discussed below.

Last but not least, there are uncertainties associated with experimental data or, in our case, with the results of NPWA used as input in our calculation, see sect. 4 for more details. In particular, we emphasize that the data base used in the NPWA of 1993 has been extended considerably since that time. Specifically, the final database below $E_{\text{lab}} = 350\,\text{MeV}$ used in the NPWA involved 1787 pp and 2514 np data. On the other hand, the database used, *e.g.*, in the construction of the CD Bonn potential [86] consists of 2932 pp and 3058 np data. We expect that increasing the experimental database should have little impact

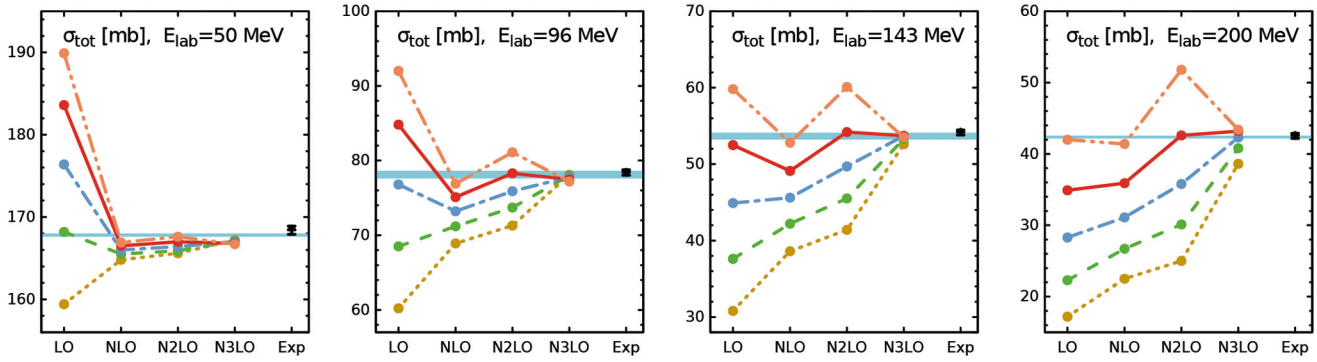

Fig. 7. (Color online) Order-by-order convergence of the chiral expansion for the np total cross section at energies of $E_{\rm lab} = 50\,$MeV, $E_{\rm lab} = 96\,$MeV and $E_{\rm lab} = 143\,$MeV and $E_{\rm lab} = 200\,$MeV. Dotted (light brown), dashed (green), dash-dotted (blue), solid (red) and dash-double-dotted (pink) lines show the results based on the cutoff $R = 1.2\,$fm, $R = 1.1\,$fm, $R = 1.0\,$fm, $R = 0.9\,$fm and $R = 0.8\,$fm, respectively. The horizontal band refers to the result of the NPWA with the uncertainty estimated by means of deviations from the results based on the Nijmegen I, II and Reid 93 potentials as explained in the text. Also shown are experimental data of ref. [113].

on the resulting phase shifts at the level of the systematic uncertainty of the NPWA assumed in our work as described in sect. 4. For example, as shown in table 3, np and pp phase shifts obtained using the CD-Bonn potential, which is constructed using the extended database, are in a very good agreement with the NPWA. Notice, however, that pp and np phase shifts and mixing angles obtained in the recent coarse-grained potential analysis of NN scattering of ref. [112] do differ significantly from the ones of the CD Bonn potential and from those of the NPWA and the Nijmegen I, II and Reid 93 potentials. This is quite surprising given that this analysis employs essentially the same pp database as the one used in the construction of the CD-Bonn potential (while the np database with 3717 data is somewhat larger). Consequently, using the phase shifts and mixing angles reported in that work results in fairly large values of $\tilde{\chi}^2$/datum defined in sect. 4, namely $\tilde{\chi}^2/\text{datum} = 4\ldots8$. Unfortunately, neither the NPWA [45] nor the coarse-grained analysis of ref. [112] provide any estimation of the systematic uncertainties so that the origin and interpretation of these discrepancies remain unclear. We do not include the results of ref. [112] in our analysis.

We now address the *systematic* uncertainty of our calculation due to the truncation of the chiral expansion. To the order we are working, we expect it to be still the dominant source of the theoretical uncertainty. Unfortunately, most of the available calculations do not address this source of uncertainty or at best estimate it by means of a residual cutoff dependence, see, *e.g.*, [5,16,35] and references therein. Such an approach, however, is well known to suffer from several deficiencies. First of all, the resulting uncertainty depends on the employed cutoff range and, therefore, shows some arbitrariness. Secondly, as already pointed out before, the residual cutoff dependence measures the contributions due to neglected contact interactions which appear only at even orders of the momentum expansion of the NN Hamiltonian. While the residual cutoff dependence of a given NN observable at LO does indeed measure the size of NLO corrections, it reflects the sensitivity to the order-Q^4 (*i.e.* N^{3}LO) contact interactions at both NLO (order-Q^2) and N^{2}LO (order-Q^3). For this reason, the uncertainty at NLO and similarly at N^{3}LO estimated in this way may be expected to be underestimated. On the other hand, given that the range of the available momentum-space cutoffs is rather limited from above both for the conceptual and practical [92] reasons, see also the discussion in sect. 3, one is forced to employ soft cutoffs in order to have a cutoff range sufficient for an estimation of the theoretical uncertainty. Such a procedure is, however, likely to induce large finite-cutoff artefacts and, therefore, to unnecessarily overestimate the true theoretical uncertainty.

To illustrate these features, consider the chiral expansion of the np total cross section at the energies of $E_{\rm lab} = 50$, 96, 143 and 200 MeV based on the interactions introduced in the previous sections as shown in fig. 7. We also show in this figure by the horizontal band the result of the NPWA with the assumed theoretical uncertainty and the experimental data of ref. [113]. The convergence pattern for the total cross section depicted in fig. 7 shows the general features one expects to see in chiral EFT: one observes fast convergence at the lowest energy which becomes increasingly slower at higher energies. Notice that the large size of higher-order corrections at the energy of $E_{\rm lab} = 200\,$MeV relative to the leading ones is actually due to the NLO contributions being smaller than expected as will be shown below. One also observes another feature which persists at all energies, namely that the size of the N^{2}LO corrections decreases with increasing the values of R. Given that the only new ingredient in the potential at N^{2}LO is the subleading TPEP, this pattern simply reflects that the TPEP is stronger cut off for soft cutoff choices.

The results shown in fig. 7 provide a good illustration of the above mentioned issues associated with the estimation of the theoretical uncertainty by means of a cutoff variation. In particular, while the spread in the predictions does, in general, decrease with the chiral order, it remains

nearly the same at NLO and N^{2}LO. Furthermore, at NLO, it misses (albeit barely) the result of the NPWA which is consistent with the expected underestimation of the theoretical uncertainty at this order. On the other hand, while the spread in the predictions based on different cutoffs is roughly consistent with the deviations between the theory and the NPWA result for the lowest energy, it appears to significantly overestimate the uncertainty of the calculation based on lower (*i.e.* harder) cutoffs R if one estimates it via the deviation between the theory and the NPWA results. This behavior at high energy suggests that the spread between the predictions for different values of R is actually governed by artefacts associated with too soft cutoffs and does not reflect the true theoretical uncertainty of chiral EFT. We, therefore, conclude that while being a useful consistency check of the calculation, cutoff variation in the employed range does not provide a reliable approach for estimating the theoretical uncertainty. As we will show below, estimating the uncertainty via the expected size of higher-order corrections, as it is common, *e.g.*, in the Goldstone boson and single-baryon sectors of chiral perturbation theory, provides a natural and more reliable approach which, in addition, has an advantage to be applicable at any fixed value of the cutoff R.

For a given observable $X(p)$, where p is the cms momentum corresponding to the considered energy, the expansion parameter in chiral EFT is given by

$$Q = \max\left(\frac{p}{\Lambda_b}, \frac{M_\pi}{\Lambda_b}\right), \tag{33}$$

where Λ_b is the breakdown scale. Based on the results presented in sects. 4 and 5, we will use $\Lambda_b = 600\,\mathrm{MeV}$ for the cutoffs $R = 0.8$, 0.9 and 1.0 fm, $\Lambda_b = 500\,\mathrm{MeV}$ for $R = 1.1\,\mathrm{fm}$ and $\Lambda_b = 400\,\mathrm{MeV}$ for $R = 1.2$ to account for the increasing amount of cutoff artefacts which is reflected by the larger values of $\tilde{\chi}^2$/datum in table 3. We have verified the consistency of the choice $\Lambda_b = 400\,\mathrm{MeV}$ for the softest cutoff $R = 1.2\,\mathrm{fm}$ by making the error plot similar to the one shown in fig. 5. We can now confront the expected size of corrections to the np total cross section at different orders in the chiral expansion with the result of the actual calculations. In particular, for the cutoff choice of $R = 0.9\,\mathrm{fm}$, we obtain

$$\begin{aligned}
\sigma_{\rm tot}(50\,\mathrm{MeV}) &= 183.6_{\mathrm{Q}^0} - 17.1_{Q^2\,(\sim 12)} + 0.5_{Q^3\,(\sim 3)} \\
&\quad -0.2_{Q^4\,(\sim 0.8)} \\
&= 166.8\,\mathrm{mb}, \\
\sigma_{\rm tot}(96\,\mathrm{MeV}) &= 84.8_{\mathrm{Q}^0} - 9.7_{Q^2\,(\sim 11)} + 3.2_{Q^3\,(\sim 4)} \\
&\quad -0.8_{Q^4\,(\sim 1.3)} \\
&= 77.5\,\mathrm{mb}, \\
\sigma_{\rm tot}(143\,\mathrm{MeV}) &= 52.5_{\mathrm{Q}^0} - 3.4_{Q^2\,(\sim 10)} + 5.1_{Q^3\,(\sim 4)} \\
&\quad -0.5_{Q^4\,(\sim 1.8)} \\
&= 53.7\,\mathrm{mb}, \\
\sigma_{\rm tot}(200\,\mathrm{MeV}) &= 34.9_{\mathrm{Q}^0} + 1.0_{Q^2\,(\sim 9)} + 6.7_{Q^3\,(\sim 5)} \\
&\quad +0.6_{Q^4\,(\sim 2.4)} \\
&= 43.2\,\mathrm{mb},
\end{aligned} \tag{34}$$

see also fig. 7, while for the softest cutoff $R = 1.2\,\mathrm{fm}$ we find

$$\begin{aligned}
\sigma_{\rm tot}(50\,\mathrm{MeV}) &= 159.4_{\mathrm{Q}^0} + 5.4_{Q^2\,(\sim 23)} + 0.8_{Q^3\,(\sim 9)} \\
&\quad +1.6_{Q^4\,(\sim 3)} = 167.2\,\mathrm{mb}, \\
\sigma_{\rm tot}(96\,\mathrm{MeV}) &= 60.2_{\mathrm{Q}^0} + 8.7_{Q^2\,(\sim 17)} + 2.4_{Q^3\,(\sim 9)} \\
&\quad +6.8_{Q^4\,(\sim 5)} = 78.1\,\mathrm{mb}, \\
\sigma_{\rm tot}(143\,\mathrm{MeV}) &= 30.8_{\mathrm{Q}^0} + 7.8_{Q^2\,(\sim 13)} + 2.8_{Q^3\,(\sim 8)} \\
&\quad +11.2_{Q^4\,(\sim 5)} = 52.6\,\mathrm{mb}, \\
\sigma_{\rm tot}(200\,\mathrm{MeV}) &= 17.2_{\mathrm{Q}^0} + 5.3_{Q^2\,(\sim 10)} + 2.5_{Q^3\,(\sim 8)} \\
&\quad +13.6_{Q^4\,(\sim 6)} = 38.6\,\mathrm{mb}.
\end{aligned} \tag{35}$$

The expected size of NLO, N^{2}LO and N^{3}LO corrections indicated in the subscripts is estimated as $(p/\Lambda_b)^2$, $(p/\Lambda_b)^3$ and $(p/\Lambda_b)^4$ times the LO result in each particular case. The cms momenta corresponding to the energies of $E_{\rm lab} = 50$, 96, 143 and 200 MeV are $p = 153\,\mathrm{MeV}$, $p = 212\,\mathrm{MeV}$, $p = 259\,\mathrm{MeV}$ and $p = 307\,\mathrm{MeV}$, respectively. Generally, the estimated size of corrections at various orders appears to be in a reasonable agreement with their actual size. The N^{3}LO corrections are smaller than expected for $R = 0.9\,\mathrm{fm}$ but turn out to be large for the cutoff $R = 1.2\,\mathrm{fm}$ at higher energies. We emphasize that it might be too optimistic to expect a convergent expansion at the energies of $E_{\rm lab} = 143$ and 200 MeV for the softest cutoff since the expansion parameter Q in these cases is larger than 0.5. Also the fact that the LO contribution at the highest energy for $R = 1.2\,\mathrm{fm}$ amounts to less than half of the total result suggests that this cutoff is not applicable at such an energy. We also observe an interesting feature that the EFT expansion actually converges faster than expected at low energy when soft cutoffs are employed, see the first line in eq. (35) and the left plot in fig. 7. This behavior becomes even more pronounced at lower energies. In fact, when increasing the r-space cutoff R, we actually continuously integrate out pion physics, and the resulting theory would gradually turn into pionless EFT if we would further soften the cutoff. At very low energies with momenta well below the pion mass, pionless EFT, which corresponds to the expansion in p/M_π, may actually be more efficient than the expansion in chiral EFT which is controlled by the parameter M_π/Λ_b.

Having tested our estimation for the breakdown scale Λ_b in the results for the np total cross section at various chiral orders, we are now in the position to estimate the theoretical uncertainty of our results at N^{3}LO. To be on a conservative side, we will ascribe the uncertainty $\Delta X^{\mathrm{N^3LO}}(p)$ of our N^{3}LO prediction $X^{\mathrm{N^3LO}}(p)$ for an observable $X(p)$ via

$$\begin{aligned}
\Delta X^{\mathrm{N^3LO}}(p) = \max\Big(&Q^5 \times \big|X^{\mathrm{LO}}(p)\big|, \\
&Q^3 \times \big|X^{\mathrm{LO}}(p) - X^{\mathrm{NLO}}(p)\big|, \\
&Q^2 \times \big|X^{\mathrm{NLO}}(p) - X^{\mathrm{N^2LO}}(p)\big|, \\
&Q \times \big|X^{\mathrm{N^2LO}}(p) - X^{\mathrm{N^3LO}}(p)\big|\Big),
\end{aligned} \tag{36}$$

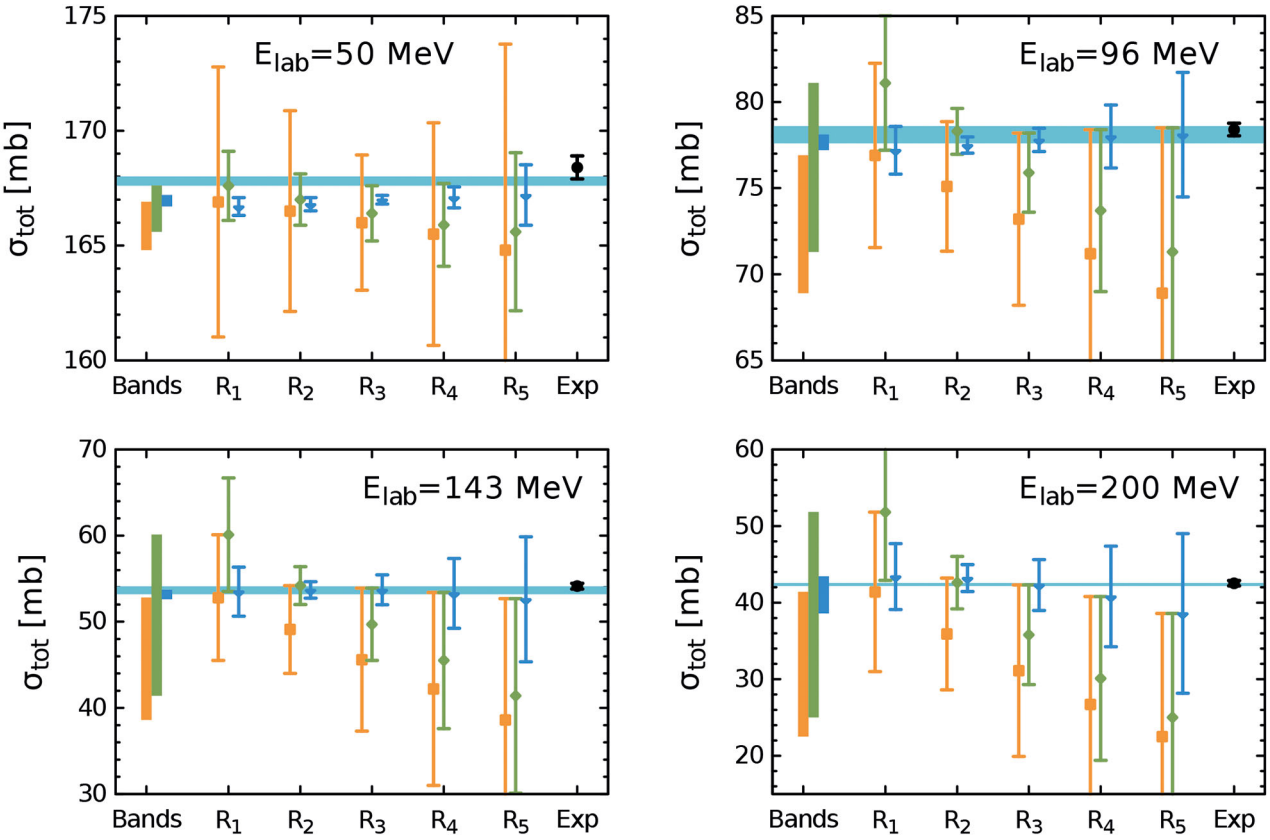

Fig. 8. (Color online) Predictions for the np total cross section based on the improved chiral NN potentials at NLO (filled squares, orange), N^{2}LO (solid diamonds, green) and N^{3}LO (filled triangles, blue) at the energies of $E_{\rm lab} = 50\,$MeV, $E_{\rm lab} = 96\,$MeV, $E_{\rm lab} = 143\,$MeV and $E_{\rm lab} = 200\,$MeV for the different choices of the cutoff: $R_1 = 0.8\,$fm, $R_2 = 0.9\,$fm, $R_3 = 1.0\,$fm, $R_4 = 1.1\,$fm, $R_5 = 1.2\,$fm. Vertical boxes depict the cutoff dependence of the theoretical predictions at different orders. The horizontal band refers to the result of the NPWA with the uncertainty estimated by means of deviations from the results based on the Nijmegen I, II and Reid 93 potentials as explained in the text. Also shown are experimental data of ref. [113].

where the expansion parameter Q is given by eq. (33) and the scale Λ_b is chosen dependent of the cutoff R as discussed above. We emphasize that such a simple estimation of the theoretical uncertainty does not provide a statistical interpretation. This can be improved, *e.g.*, by employing a Bayesian framework [93, 99] and performing marginalization over higher-order corrections. We postpone such an analysis for a future study and will adopt the simplified treatment introduced above here and in what follows. We will further impose an additional constraint for the theoretical uncertainties at NLO and N^{2}LO by requiring them to have at least the size of the actual higher-order contributions. We emphasize that the above way of estimating the uncertainty does not rely on cutoff variation and can be carried out for any given value of R.

Our results for the np total cross section at various orders in the chiral expansion and for various choices of the cutoff R are shown in fig. 8. Notice that at the smallest energy, we observe deviations between our N^{3}LO results and the NPWA which are likely caused by the employed treatment of IB corrections in the ^{1}S$_0$ partial way. In particular, we chose to determine the LECs C_{1S0}, D^1_{1S0} and D^2_{1S0} solely from the pp phase shift and adjusted $\tilde{C}^{\rm np}_{1S0}$ to reproduce the np scattering length. The splitting between the np and pp ^{1}S$_0$ phase shifts thus comes out as a prediction. It is therefore not surprising that the results for the np ^{1}S$_0$ phase shifts show some deviations from the NPWA. These deviations are expected to be largely reduced at next-higher order in the chiral expansion.

In all cases shown in fig. 8, the predicted results calculated using different values of the cutoff R agree with each other within the theoretical uncertainty. It is comforting to see that our procedure for estimating the uncertainty yields the pattern which is qualitatively similar to the one found based on the $\tilde{\chi}^2$/datum for the description of the Nijmegen np and pp phase shifts as shown in table 3. In particular, we see that the most accurate results at the lowest energy are achieved with the cutoff $R = 1.0\,$fm (with the uncertainty for the $R = 0.9\,$fm case being of a comparable size). At higher energies, the cutoff $R = 0.9\,$fm clearly provides the most accurate choice. We also observe that at the lowest energy, the cutoff variation does considerably underestimate the theoretical uncertainty at NLO and, to a lesser extent, at N^{3}LO as expected based on the arguments given above. This pattern changes at higher energies. For

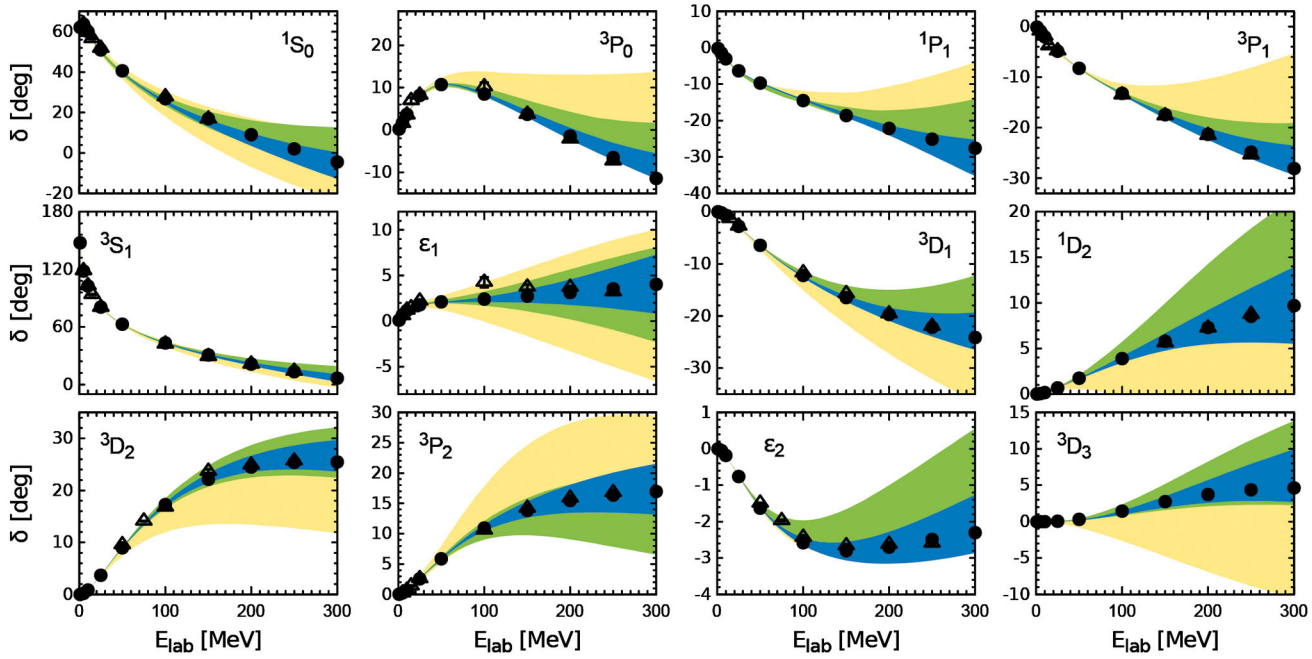

Fig. 9. (Color online) Estimated theoretical uncertainty of the np phase shifts at NLO, N^{2}LO and N^{3}LO based on the cutoff of $R = 0.9\,\text{fm}$ in comparison with the NPWA [45] (solid dots) and the GWU single-energy np partial wave analysis [94] (open triangles). The light-(yellow), medium-(green) and dark-(blue) shaded bands depict the estimated theoretical uncertainties at NLO, N^{2}LO and N^{3}LO, as explained in the text. Only those partial waves are shown which have been used in the fits at N^{3}LO.

example, at $E_{\text{lab}} = 200\,\text{MeV}$, the cutoff bands at NLO and N^{3}LO appear to be of the same size as the estimated uncertainty based on the optimal cutoff $R = 0.9\,\text{fm}$. It is actually a combination of two effects which work against each other which results in a "reasonable" estimation of the NLO and N^{3}LO uncertainties at higher energies by the cutoff bands: on the one hand, as already mentioned above, cutoff bands measure the impact of the order-Q^4 and order-Q^6 contact interactions and, therefore, underestimate the uncertainty at NLO and N^{3}LO. On the other hand, at higher energies, cutoff bands get increased due to using softer values of R as it is clearly visible from fig. 8. This conclusion is further supported by the N^{2}LO cutoff band which strongly overestimates the estimated uncertainty in the case of $R = 0.9\,\text{fm}$. We also learn from fig. 8 that N^{2}LO results for the total cross section for the cutoffs of $R = 0.9\,\text{fm}$ and $R = 1.0\,\text{fm}$ have the accuracy which is comparable to N^{3}LO calculations with the softest cutoff $R = 1.2\,\text{fm}$. In summary, we find that the suggested approach for error estimation is more reliable than the standard procedure by means of cutoff bands and, in addition, has the advantage of being applicable for a fixed value of R. This allows one to avoid the artificial increase of the theoretical uncertainty due to cutoff artefacts, the issue which is especially relevant at high energies where the chiral expansion converges slower. The issue with using the cutoff bands is expected to become particularly important at next-to-next-to-next-to-next-to-leading order (N^{4}LO) in the chiral expansion. In particular, we expect that the residual cutoff dependence at N^{4}LO will be comparable to that at N^{3}LO, and that it will significantly overestimate the real N^{4}LO uncertainty at higher energies in a close analogy to what is observed at N^{2}LO. Last but not least, the ability to carry out independent calculations with quantified uncertainties also provides a useful consistency check.

Next, we show in fig. 9 the estimated uncertainty of the S-, P- and D-wave phase shifts and the mixing angles ϵ_1 and ϵ_2 at NLO, N^{2}LO and N^{3}LO based on $R = 0.9\,\text{fm}$. The various bands result by adding/subtracting the estimated theoretical uncertainty, $\pm\Delta\delta(E_{\text{lab}})$ and $\pm\Delta\epsilon(E_{\text{lab}})$, to/from the results shown in fig. 3. In a similar way, we also looked at selected neutron-proton scattering observables at different energies shown in figs. 10–13. For the lowest considered energy of $E_{\text{lab}} = 50\,\text{MeV}$, we show, in addition to the results using $R = 0.9\,\text{fm}$, also our predictions for the softest cutoff choice of $R = 1.2\,\text{fm}$. While the uncertainty is clearly increased, the results actually still appear to be rather accurate at this energy. Our results agree with the ones of the NPWA for all considered observables and energies indicating that the employed way to estimate the uncertainties is quite reliable. Generally, we find that chiral EFT at N^{3}LO allows for very accurate results at energies below $E_{\text{lab}} \sim 100\,\text{MeV}$ and still provides accurate description of the data at energies of the order of $E_{\text{lab}} \sim 200\,\text{MeV}$. These findings are particularly promising for the ongoing studies of the three-nucleon force whose contributions to nucleon-deuteron scattering observables are believed to increase at energies above $E_{\text{N, lab}} \sim 100\,\text{MeV}$. It would be interesting to perform a similar analysis of nucleon-deuteron scattering data based on the improved chiral NN potentials in order to see whether accurate predictions are to be expected at such energies at N^{3}LO. Work along these lines is in progress.

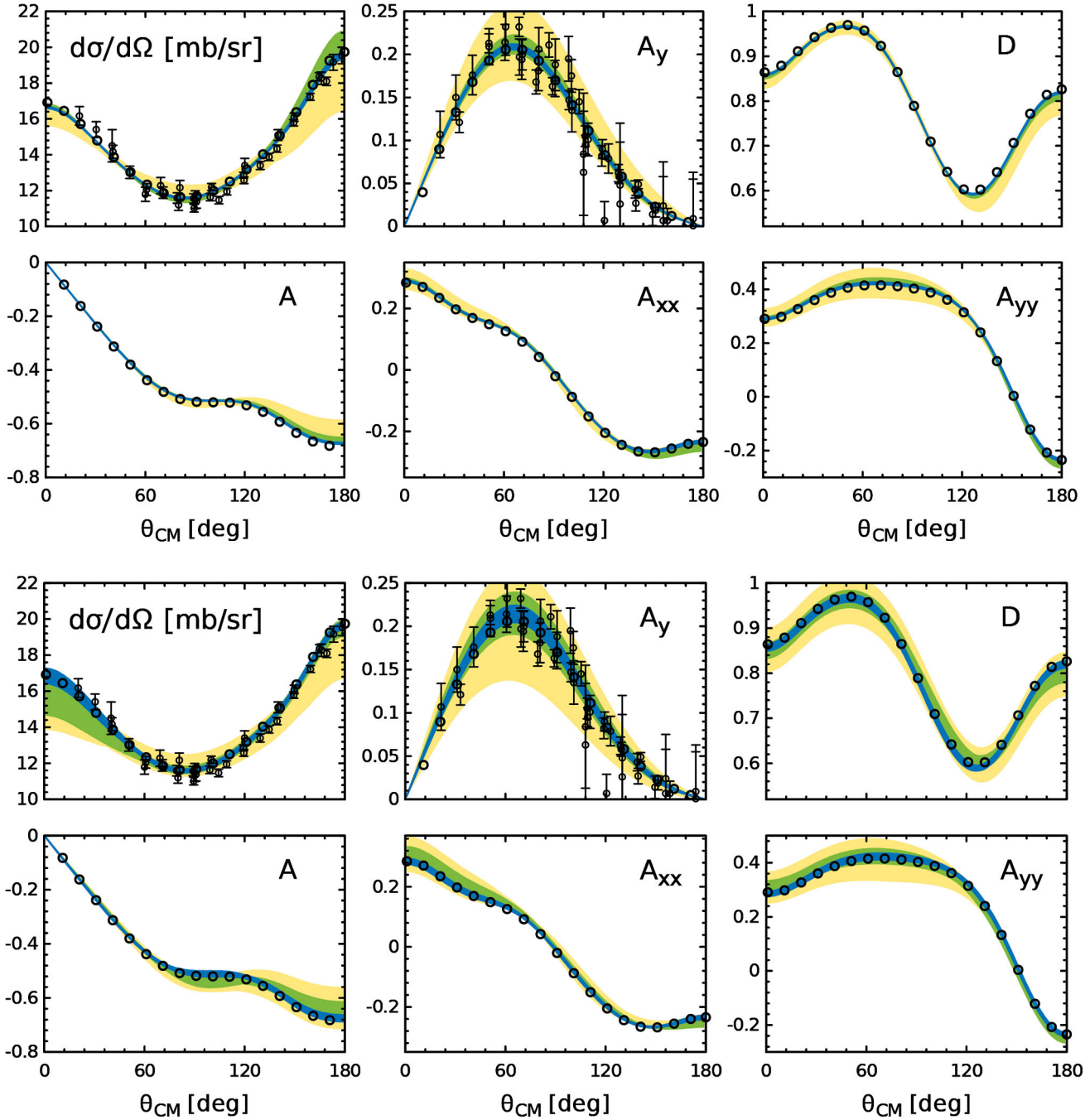

Fig. 10. (Color online) Estimated theoretical uncertainty of the chiral EFT results for np differential cross section $\mathrm{d}\sigma/\mathrm{d}\Omega$, vector analyzing power A, polarization transfer coefficients D and A and spin correlation parameters A_{xx} and A_{yy} at laboratory energy of $E_{\mathrm{lab}} = 50\,\mathrm{MeV}$. The light-(yellow), medium-(green) and dark-(blue) shaded bands depict the estimated theoretical uncertainties at NLO, $\mathrm{N^2LO}$ and $\mathrm{N^3LO}$, respectively. Open circles refer to the result of the NPWA. The upper (lower) panel shows the results based on the optimal (softest) cutoff choice of $R = 0.9\,\mathrm{fm}$ ($R = 1.2\,\mathrm{fm}$). Data for the cross section are taken from [114, 115] and for the analyzing power from [116–120].

The formulated approach for error estimation can be straightforwardly applied to the deuteron properties as well. For example, one finds for the optimal cutoff choice of $R = 0.9\,\mathrm{fm}$ the uncertainty of the asymptotic S state normalization A_S to be $\sim 0.013\,\mathrm{fm}^{-1/2}$ at NLO, $\sim 0.003\,\mathrm{fm}^{-1/2}$ at $\mathrm{N^2LO}$ and $\sim 0.0008\,\mathrm{fm}^{-1/2}$ at $\mathrm{N^3LO}$. The uncertainty of the D/S state ratio η is estimated to be ~ 0.001 at NLO, ~ 0.0003 at $\mathrm{N^2LO}$ and ~ 0.0001 at $\mathrm{N^3LO}$. Here we have assumed that the expansion parameter is given by $Q = M_\pi/\Lambda_b$. For both observables, the theoretical uncertainties at $\mathrm{N^3LO}$ already appear to be below the ones of the empirical numbers.

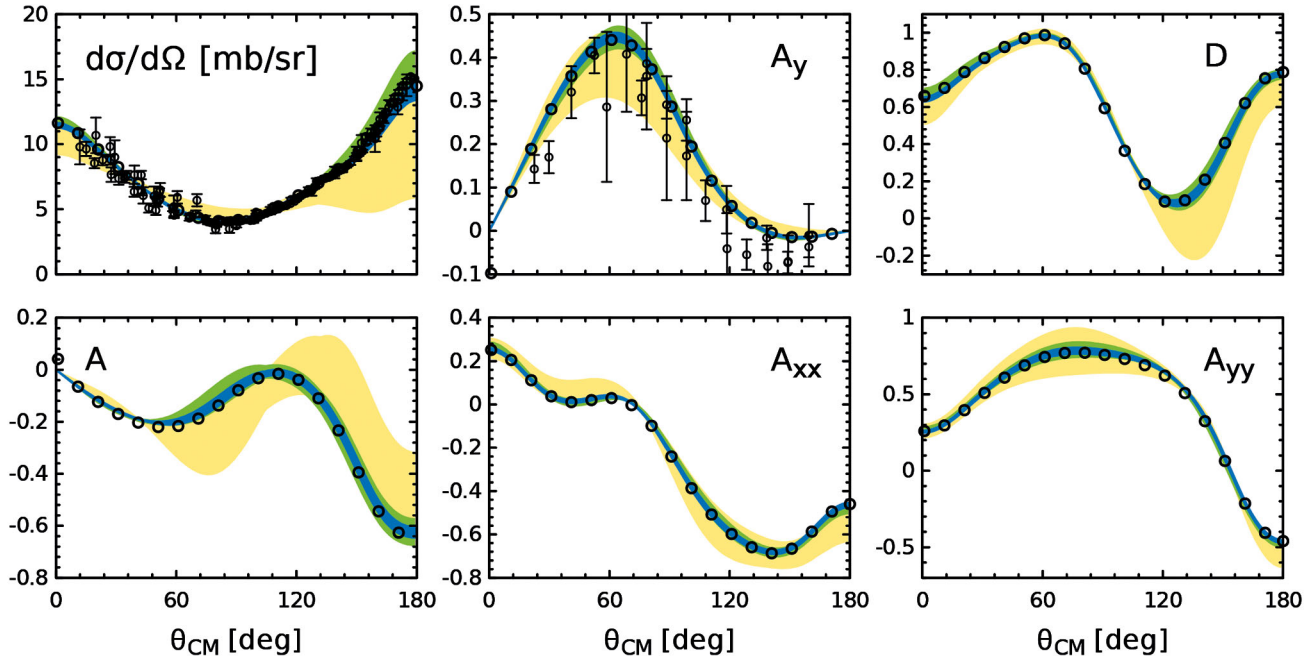

Fig. 11. Estimated theoretical uncertainty of the chiral EFT results for np differential cross section $\mathrm{d}\sigma/\mathrm{d}\Omega$, vector analyzing power A, polarization transfer coefficients D and A and spin correlation parameters A_{xx} and A_{yy} at laboratory energy of $E_{\mathrm{lab}} = 96\,\mathrm{MeV}$ calculated using on the cutoff of $R = 0.9\,\mathrm{fm}$. The light-(yellow), medium-(green) and dark-(blue) shaded bands depict the estimated theoretical uncertainties at NLO, $\mathrm{N^2LO}$ and $\mathrm{N^3LO}$, respectively. Open circles refer to the result of the NPWA. Data for the cross section are taken from [121–123]. Data for the analyzing power are at $E_{\mathrm{lab}} = 95\,\mathrm{MeV}$ and taken from [124].

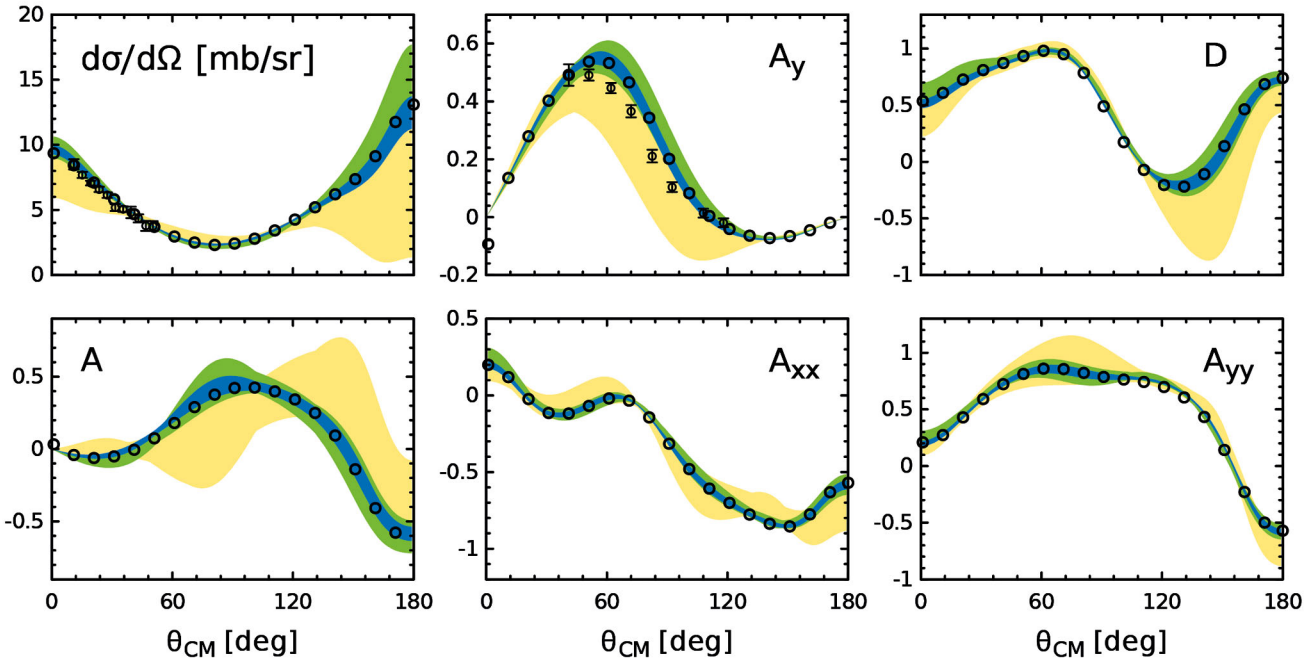

Fig. 12. (Color online) Estimated theoretical uncertainty of the chiral EFT results for np differential cross section $\mathrm{d}\sigma/\mathrm{d}\Omega$, vector analyzing power A, polarization transfer coefficients D and A and spin correlation parameters A_{xx} and A_{yy} at laboratory energy of $E_{\mathrm{lab}} = 143\,\mathrm{MeV}$ calculated using on the cutoff of $R = 0.9\,\mathrm{fm}$. The light-(yellow), medium-(green) and dark-(blue) shaded bands depict the estimated theoretical uncertainties at NLO, $\mathrm{N^2LO}$ and $\mathrm{N^3LO}$, respectively. Open circles refer to the result of the NPWA. Data for the cross section are at $E_{\mathrm{lab}} = 142.8\,\mathrm{MeV}$ and taken from [125] and for the analyzing power from [126].

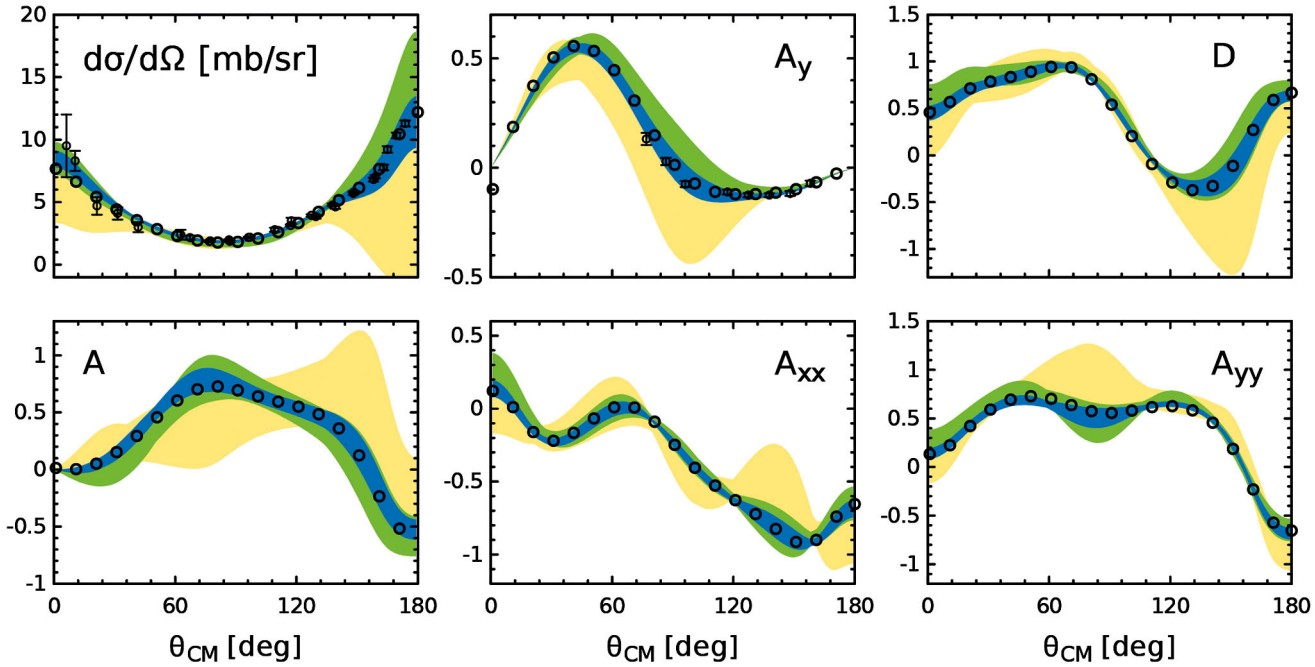

Fig. 13. (Color online) Estimated theoretical uncertainty of the chiral EFT results for np differential cross section $\mathrm{d}\sigma/\mathrm{d}\Omega$, vector analyzing power A, polarization transfer coefficients D and A and spin correlation parameters A_{xx} and A_{yy} at laboratory energy of $E_{\rm lab} = 200\,\mathrm{MeV}$ calculated using on the cutoff of $R = 0.9\,\mathrm{fm}$. The light-(yellow), medium-(green) and dark-(blue) shaded bands depict the estimated theoretical uncertainties at NLO, N^{2}LO and N^{3}LO, respectively. Open circles refer to the result of the NPWA. Data for the cross section are at $E_{\rm lab} = 199\,\mathrm{MeV}$ from [127] and at $E_{\rm lab} = 200\,\mathrm{MeV}$ from [128]. Data for the analyzing power are at $E_{\rm lab} = 199\,\mathrm{MeV}$ from [127].

Finally, we emphasize that our results depend little on the specific choice of the regulator function. In order to quantify this dependence, we performed fits using the cutoff $R = 1.0\,\mathrm{fm}$ but employing different values of the exponent in eq. (27), namely $n = 5$ and $n = 7$. In table 7, we show the resulting phase shifts in the ^{3}S$_1$ and pp ^{1}S$_0$, ^{3}P$_0$, ^{3}P$_1$ and ^{3}P$_2$ partial waves at the energies of 10, 100 and 200 MeV as representative examples. Clearly, the observed spread in the results is negligibly small compared to the estimated accuracy of our calculations. Furthermore, as already pointed out in sect. 3, the employed local regularization of the pion-exchange contributions makes the spectral function regularization obsolete. In particular, phase shifts resulting from fits using different values of the SFR cutoff $\Lambda = 1\,\mathrm{GeV}$, $\Lambda = 1.5\,\mathrm{GeV}$ and $\Lambda = 2\,\mathrm{GeV}$, see the last three columns in table 7, are nearly indistinguishable from each other and from the DR result corresponding to $\Lambda = \infty$ and shown in the third column of this table.

8 Summary and conclusions

In this paper we have presented a new generation of NN potentials derived in chiral EFT up to N^{3}LO[9]. The new chiral forces offer a number of substantial improvements as compared to the widely used N^{3}LO potentials of refs. [16,17] introduced a decade ago. First of all, we employ a local regularization scheme for the pion exchange contributions which, differently to the standard nonlocal regularization applied, *e.g.*, in refs. [16,17], does not distort the low-energy analytic structure of the amplitude and, as a consequence, leads to a better description of phase shifts and experimental data. The employed regulator, by construction, removes the short-range part of the chiral two-pion exchange and thus makes the additional spectral function regularization used in the potential of ref. [16] obsolete. This is a particularly welcome feature given that the expressions for the three-nucleon force at N^{3}LO and N^{4}LO are only available in the framework of dimensional regularization. Further, in contrast to the earlier studies of refs. [16,17], we have taken all pion-nucleon LECs and especially the subleading LECs c_i from pion-nucleon scattering without any fine tuning. The LECs accompanying NN contact interactions were determined by fits to the Nijmegen phase shifts and mixing angles for five different values of the coordinate-space cutoff R chosen in the range of $R = 0.8\ldots1.2\,\mathrm{fm}$ and appear to be of natural size in all cases. The new N^{3}LO potentials allow for an excellent description of the Nijmegen np and pp phase shifts at energies below 200 MeV and, for the cutoff choices of $R = 0.9\,\mathrm{fm}$ and $R = 1.0\,\mathrm{fm}$, even up to $E_{\rm lab} = 300\,\mathrm{MeV}$. Furthermore, the deuteron properties are accurately described. Moreover, the deuteron wave functions are free from distortions at distances larger than $r \sim 2\ldots3\,\mathrm{fm}$ which appear for the N^{3}LO potentials of refs. [16,17] due

[9] A user-friendly computer program to generate matrix elements of the new chiral potentials will be made available upon request after completing the testing phase.

Table 7. Selected phase shifts (in degrees) calculated at N^{3}LO using the cutoff of $R = 1.0\,\text{fm}$ with the theoretical uncertainty determined according to eq. (36) in comparison with the results of the NPWA. Also shown are N^{3}LO fits for the same value of R but a different functional form of the regulator with $n = 5$ and $n = 7$, see eq. (27), and fits based on the spectral function regularization with the corresponding cutoff of $\Lambda = 1\,\text{GeV}$, $\Lambda = 1.5\,\text{GeV}$ and $\Lambda = 2\,\text{GeV}$.

Lab. energy	NPWA [45]	Our result	DR, $n = 5$	DR, $n = 7$	SFR, 1.0 GeV	SFR, 1.5 GeV	SFR, 2.0 GeV
Proton-proton $^1S_0$ phase shift							
10 MeV	55.23	55.22 ± 0.08	55.22	55.22	55.22	55.22	55.22
100 MeV	24.99	24.98 ± 0.60	24.98	24.98	24.98	24.98	24.98
200 MeV	6.55	6.56 ± 2.2	6.55	6.56	6.56	6.56	6.57
Neutron-proton $^3S_1$ phase shift							
10 MeV	102.61	102.61 ± 0.07	102.61	102.61	102.61	102.61	102.61
100 MeV	43.23	43.22 ± 0.30	43.28	43.20	43.17	43.21	43.22
200 MeV	21.22	21.2 ± 1.4	21.2	21.2	21.2	21.2	21.2
Proton-proton $^3P_0$ phase shift							
10 MeV	3.73	3.75 ± 0.04	3.75	3.75	3.75	3.75	3.75
100 MeV	9.45	9.17 ± 0.30	9.15	9.18	9.18	9.17	9.17
200 MeV	−0.37	-0.1 ± 2.3	−0.1	−0.1	−0.1	−0.1	−0.1
Proton-proton $^3P_1$ phase shift							
10 MeV	−2.06	-2.04 ± 0.01	−2.04	−2.04	−2.04	−2.04	−2.04
100 MeV	−13.26	-13.42 ± 0.17	−13.43	−13.41	−13.41	−13.42	−13.42
200 MeV	−21.25	-21.2 ± 1.6	−21.2	−21.2	−21.2	−21.2	−21.2
Proton-proton $^3P_2$ phase shift							
10 MeV	0.65	0.65 ± 0.01	0.66	0.65	0.65	0.65	0.65
100 MeV	11.01	11.03 ± 0.50	10.97	11.06	11.07	11.05	11.04
200 MeV	15.63	15.6 ± 1.9	15.6	15.5	15.5	15.5	15.6

to the employed form of the regulator. We found that the description of the Nijmegen phase shifts improves substantially when going from LO to NLO, from NLO to N^{2}LO and from N^{2}LO to N^{3}LO as one expects for a convergent expansion. It is worth to emphasize in this connection that the short range part of the NLO and N^{2}LO potentials involves the same set of operators. Our findings therefore provide yet another evidence of the subleading two-pion exchange which was also observed in earlier studies. As an important consistency check of our approach, we have studied the residual cutoff dependence of phase shifts at different orders in the chiral expansion. We found, in particular, that the cutoff dependence is strongly reduced at N^{3}LO compared to N^{2}LO in the whole considered range of energies.

We have also addressed the issue of the uncertainty of our results due to the truncation of the chiral expansion at a given order. In particular, we have argued that the standard procedure for error estimation based on a cutoff variation is not reliable and employed a simple alternative approach by directly estimating the expected size of higher-order contributions at a given energy. Such a procedure has the advantage of being applicable for any fixed value of the cutoff so that calculations based on different cutoffs can be used to provide additional consistency checks. Furthermore, disentangling the error analysis from the cutoff variation allows one to avoid an unnecessary increase of uncertainty due to softening the interaction. Notice that the versions of the potential corresponding to soft choices of the cutoff R may still be useful for certain kinds of applications including, in particular, many-body calculations. We have applied this approach to the total np cross section at several energies and have verified that the results at different chiral orders and for different values of the cutoff are indeed consistent with each other. We have furthermore used this method to quantify the theoretical uncertainty in the description of the np phase shifts as well as differential cross sections and selected polarization observables in np scattering. In particular, we found the N^{3}LO results for np scattering to be very accurate at energies below $\sim 100\,\text{MeV}$ with the corresponding error bands being barely visible and still rather accurate at the energy of $E_{\text{lab}} = 200\,\text{MeV}$. In all considered cases, our results agree with the ones based on the NPWA within the estimated theoretical accuracy. This gives us additional confidence in the reliability of the suggested way of quantifying the uncertainty. We have furthermore analyzed the uncertainties associated with making a specific choice of the functional form of the local regulator and employing the additional spectral function regularization of the TPEP and found them to be negligible at the level of the estimated theoretical accuracy at N^{3}LO.

The improved chiral potentials introduced in this work should provide an excellent starting point for applications

to few-nucleon systems. In particular, nucleon-deuteron scattering offers a natural testing ground for studying the details of the three-nucleon force which is subject of extensive research [15]. The existing calculations based on modern phenomenological potentials suggest that effects of the three-nucleon force in nucleon-deuteron scattering should be small at low energy (except for certain observables like the vector analyzing power) but become clearly visible at intermediate energies of $E_{\rm N,\,lab} \sim 70\,$MeV and above. It is encouraging to see that chiral EFT provides a rather accurate description of NN scattering in this energy range. We expect a similar theoretical accuracy for nucleon-deuteron scattering observables, but this needs to be verified via explicit calculations. Work along these lines is in progress. For applications to medium-mass and heavy nuclei based on the continuum methods, the potentials typically need to be softened by using the renormalization group type techniques such as, *e.g.*, the similarity renormalization group approach, in order to make the many-body problem numerically tractable. It remains to be seen whether the new NN potentials, which do have a substantial amount of high-momentum components due to the employed local regulator, can be softened sufficiently without inducing a too large amount of many-body forces.

In addition to the already mentioned applications to few- and many-nucleon systems, this work should be extended in various directions. First, the calculations should be carried out at next-higher order in the chiral expansion, see ref. [95] for a recent work along this line. This would, in particular, provide a nontrivial check for our estimation of uncertainties at N^{3}LO. Secondly, isospin-breaking effects and the role of the three-pion exchange contributions should be studied in detail. Furthermore, it is important to quantify the uncertainty associated with the values of the pion-nucleon LECs and investigate the possibility of constraining them from NN or even few-nucleon data in a systematic way. Last but not least, it would be desirable to employ a more elaborate way of estimating the systematic theoretical uncertainty which would allow for a statistical interpretation of the errors. Work along these lines is in progress.

We are grateful to Dick Furnstahl for careful reading of the manuscript and for many useful comments and suggestions. This work was supported by the European Community-Research Infrastructure Integrating Activity "Study of Strongly Interacting Matter" (acronym HadronPhysics3, Grant Agreement n. 283286) under the Seventh Framework Programme of EU, the ERC project 259218 NUCLEAREFT and by the DFG and NSFC (CRC 110).

Appendix A. Scattering amplitude in the partial wave basis

Consider two nucleons moving with momenta $\vec{p}_1$ and $\vec{p}_2$. We use relativistic kinematics for relating the energy $E_{\rm lab}$ of the two nucleons in the laboratory system to the square of the nucleon momentum $\vec{p}$ in the cms defined by the condition $\vec{p}_1 + \vec{p}_2 = 0$. As explained in sect. 2, the NN potentials constructed in the present work are to be used in the Schrödinger equation[10]

$$\left[\frac{p^2}{m_N} + V\right]\Psi = \frac{k^2}{m_N}\Psi. \tag{A.1}$$

where $m_N = m_p$, $m_N = m_n$ and $m_N = 2m_p m_n/(m_p + m_n)$ for the pp, nn and np systems, respectively. Here and in what follows we use for all momenta the notation of, *e.g.*, $p \equiv |\vec{p}|$. The relation between $E_{\rm lab}$ and k^2 in the above equation is based on relativistic kinematics and reads

– Proton-proton case:

$$k^2 = \frac{1}{2} m_p E_{\rm lab}\,. \tag{A.2}$$

– Neutron-neutron case:

$$k^2 = \frac{1}{2} m_n E_{\rm lab}\,. \tag{A.3}$$

– Neutron-proton case:

$$k^2 = \frac{m_p^2 E_{\rm lab}(E_{\rm lab} + 2m_n)}{(m_n + m_p)^2 + 2E_{\rm lab} m_p}\,. \tag{A.4}$$

The Lippmann-Schwinger equation for the off-the-energy shell T-matrix corresponding to eq. (A.1) and projected onto states with orbital angular momentum l, total spin s and total angular momentum j has the form

$$T^{sj}_{l'l}(p', p; k^2) = V^{sj}_{l'l}(p', p) + \sum_{l''} \int_0^\infty {\rm d}q\, q^2\, V^{sj}_{l'l''}(p', q) \times \frac{m_N}{k^2 - q^2 + i\eta} T^{sj}_{l''l}(q, p; k^2), \tag{A.5}$$

with $\eta \to 0^+$. In the uncoupled case, l is conserved. The partial wave projected potential $V^{sj}_{ll'}(p', p)$ can be obtained using the formulae collected in appendix B of ref. [16]. The relation between the S- and T-matrices is given by

$$S^{sj}_{l'l}(k) = \delta_{l'l} - i\pi k m_N T^{sj}_{l'l}(k, k; k^2). \tag{A.6}$$

The phase shifts in the uncoupled cases can be obtained from the S-matrix via

$$S^{0j}_{jj} = \exp\left(2i\delta^{0j}_j\right), \qquad S^{1j}_{jj} = \exp\left(2i\delta^{1j}_j\right), \tag{A.7}$$

where we have used the notation δ^{sj}_l. Throughout, we use the so-called Stapp parametrization [129] of the S-matrix in the coupled channels ($j > 0$) defined as

$$S = \begin{pmatrix} S^{1j}_{j-1\,j-1} & S^{1j}_{j-1\,j+1} \\ S^{1j}_{j+1\,j-1} & S^{1j}_{j+1\,j+1} \end{pmatrix} = \begin{pmatrix} \cos(2\epsilon)\exp(2i\delta^{1j}_{j-1}) & i\sin(2\epsilon)\exp(i\delta^{1j}_{j-1} + i\delta^{1j}_{j+1}) \\ i\sin(2\epsilon)\exp(i\delta^{1j}_{j-1} + i\delta^{1j}_{j+1}) & \cos(2\epsilon)\exp(2i\delta^{1j}_{j+1}) \end{pmatrix}, \tag{A.8}$$

[10] For the np system, this equation is correct modulo terms which are proportional to $(m_p - m_n)^2$ which are beyond the accuracy of the present calculation.

and is related to another frequently used parametrization due to Blatt and Biedenharn [130, 131] in terms of $\tilde{\delta}$ and $\tilde{\epsilon}$ via the following equations:

$$\begin{aligned} \delta_{j-1} + \delta_{j+1} &= \tilde{\delta}_{j-1} + \tilde{\delta}_{j+1}, \\ \sin(\delta_{j-1} - \delta_{j+1}) &= \frac{\tan(2\epsilon)}{\tan(2\tilde{\epsilon})}, \\ \sin(\tilde{\delta}_{j-1} - \tilde{\delta}_{j+1}) &= \frac{\sin(2\epsilon)}{\sin(2\tilde{\epsilon})}. \end{aligned} \tag{A.9}$$

For pp scattering, the phase shifts considered in the present work are of the nuclear plus relativistic Coulomb interaction with respect to relativistic Coulomb wave functions, *i.e.* δ^{C1}_{C1+N} using the notation of ref. [45]. We use the method proposed by Vincent and Phatak [132] to calculate the corresponding phase shifts and mixing angles in momentum space, see also refs. [16,40,86] for a description of this approach.

References

1. S.R. Beane, W. Detmold, K. Orginos, M.J. Savage, Prog. Part. Nucl. Phys. **66**, 1 (2011) arXiv:1004.2935 [hep-lat].
2. S. Weinberg, Phys. Lett. B **251**, 288 (1990).
3. U. van Kolck, Phys. Rev. C **49**, 2932 (1994).
4. C. Ordonez, L. Ray, U. van Kolck, Phys. Rev. C **53**, 2086 (1996) hep-ph/9511380.
5. E. Epelbaum, H.W. Hammer, U.-G. Meißner, Rev. Mod. Phys. **81**, 1773 (2009) arXiv:0811.1338 [nucl-th].
6. N. Kalantar-Nayestanaki, E. Epelbaum, J.G. Messchendorp, A. Nogga, Rep. Prog. Phys. **75**, 016301 (2012) arXiv:1108.1227 [nucl-th].
7. H.W. Hammer, A. Nogga, A. Schwenk, Rev. Mod. Phys. **85**, 197 (2013) arXiv:1210.4273 [nucl-th].
8. J.W. Holt, N. Kaiser, W. Weise, Prog. Part. Nucl. Phys. **73**, 35 (2013) arXiv:1304.6350 [nucl-th].
9. J.P. Vary, Nucl. Phys. Proc. Suppl. **251**, 155 (2014).
10. H. Krebs, A. Gasparyan, E. Epelbaum, Phys. Rev. C **87**, 054007 (2013) arXiv:1302.2872 [nucl-th].
11. D.R. Phillips, C. Schat, Phys. Rev. C **88**, 034002 (2013) arXiv:1307.6274 [nucl-th].
12. E. Epelbaum, A.M. Gasparyan, H. Krebs, C. Schat, arXiv:1411.3612 [nucl-th].
13. R. Machleidt, D.R. Entem, J. Phys. G **37**, 064041 (2010) arXiv:1001.0966 [nucl-th].
14. E. Epelbaum, in *Proceedings of the 10th Conference on Quark Confinement and the Hadron Spectrum (Confinement X) Munich, Germany, October 8–12, 2012*, edited by Matthias Berwein, Nora Brambilla, Stephan Paul (2012) 014, arXiv:1302.3241 [nucl-th].
15. Low-Energy Nuclear Physics International Collaboration, `http://www.lenpic.org`.
16. E. Epelbaum, W. Glöckle, U.-G. Meißner, Nucl. Phys. A **747**, 362 (2005) nucl-th/0405048.
17. D.R. Entem, R. Machleidt, Phys. Rev. C **68**, 041001 (2003) nucl-th/0304018.
18. E. Epelbaum, W. Glöckle, U.-G. Meißner, Eur. Phys. J. A **19**, 125 (2004) nucl-th/0304037.
19. E. Epelbaum, W. Glöckle, U.-G. Meißner, Eur. Phys. J. A **19**, 401 (2004) nucl-th/0308010.
20. R. Machleidt, D.R. Entem, Phys. Rep. **503**, 1 (2011) arXiv:1105.2919 [nucl-th].
21. V. Bernard, N. Kaiser, U.-G. Meißner, Nucl. Phys. A **615**, 483 (1997) hep-ph/9611253.
22. A. Manohar, H. Georgi, Nucl. Phys. B **234**, 189 (1984).
23. G.P. Lepage, nucl-th/9706029.
24. S.R. Beane, P.F. Bedaque, M.J. Savage, U. van Kolck, Nucl. Phys. A **700**, 377 (2002) nucl-th/0104030.
25. A. Nogga, R.G.E. Timmermans, U. van Kolck, Phys. Rev. C **72**, 054006 (2005) nucl-th/0506005.
26. B. Long, C.J. Yang, Phys. Rev. C **85**, 034002 (2012) arXiv:1111.3993 [nucl-th].
27. M.C. Birse, Philos. Trans. R. Soc. London A **369**, 2662 (2011) arXiv:1012.4914 [nucl-th].
28. M. Pavon Valderrama, Phys. Rev. C **84**, 064002 (2011) arXiv:1108.0872 [nucl-th].
29. E. Epelbaum, U.-G. Meißner, Few-Body Syst. **54**, 2175 (2013) nucl-th/0609037.
30. E. Epelbaum, J. Gegelia, Eur. Phys. J. A **41**, 341 (2009) arXiv:0906.3822 [nucl-th].
31. E. Epelbaum, J. Gegelia, Phys. Lett. B **716**, 338 (2012) arXiv:1207.2420 [nucl-th].
32. E. Epelbaum, A.M. Gasparyan, J. Gegelia, H. Krebs, arXiv:1501.01191 [nucl-th].
33. N. Kaiser, R. Brockmann, W. Weise, Nucl. Phys. A **625**, 758 (1997) nucl-th/9706045.
34. E. Epelbaum, W. Glöckle, U.-G. Meißner, Nucl. Phys. A **637**, 107 (1998) nucl-th/9801064.
35. E. Epelbaum, Prog. Part. Nucl. Phys. **57**, 654 (2006) nucl-th/0509032.
36. E. Epelbaum, Eur. Phys. J. A **34**, 197 (2007) arXiv: 0710.4250 [nucl-th].
37. E. Epelbaum, arXiv:1001.3229 [nucl-th].
38. U. van Kolck, M.C.M. Rentmeester, J.L. Friar, J.T. Goldman, J.J. de Swart, Phys. Rev. Lett. **80**, 4386 (1998) nucl-th/9710067.
39. J.L. Friar, U. van Kolck, Phys. Rev. C **60**, 034006 (1999) nucl-th/9906048.
40. M. Walzl, U.-G. Meißner, E. Epelbaum, Nucl. Phys. A **693**, 663 (2001) nucl-th/0010019.
41. J.L. Friar, U. van Kolck, G.L. Payne, S.A. Coon, Phys. Rev. C **68**, 024003 (2003) nucl-th/0303058.
42. E. Epelbaum, U.-G. Meißner, Phys. Rev. C **72**, 044001 (2005) nucl-th/0502052.
43. N. Kaiser, Phys. Rev. C **73**, 064003 (2006) nucl-th/0605040.
44. J.J. de Swart, M.C.M. Rentmeester, R.G.E. Timmermans, PiN Newslett. **13**, 96 (1997) nucl-th/9802084.
45. V.G.J. Stoks, R.A.M. Klomp, M.C.M. Rentmeester, J.J. de Swart, Phys. Rev. C **48**, 792 (1993) Nijmegen NN online program, `http://nn-online.org/`.
46. N. Kaiser, Phys. Rev. C **64**, 057001 (2001) nucl-th/0107064.
47. N. Fettes, U.-G. Meißner, S. Steininger, Nucl. Phys. A **640**, 199 (1998) hep-ph/9803266.
48. S. Weinberg, Nucl. Phys. B **363**, 3 (1991).
49. J.L. Friar, Phys. Rev. C **60**, 034002 (1999) nucl-th/9901082.
50. V. Bernard, E. Epelbaum, H. Krebs, U.-G. Meißner, Phys. Rev. C **84**, 054001 (2011) arXiv:1108.3816 [nucl-th].
51. E. Epelbaum, J. Gegelia, PoS CD **12**, 090 (2013) arXiv:1301.6134 [nucl-th].

52. E. Epelbaum, A.M. Gasparyan, J. Gegelia, M.R. Schindler, Eur. Phys. J. A **50**, 51 (2014) arXiv:1311.7164 [nucl-th].
53. E. Marji, A. Canul, Q. MacPherson, R. Winzer, C. Zeoli, D.R. Entem, R. Machleidt, Phys. Rev. C **88**, 054002 (2013) arXiv:1309.5114 [nucl-th].
54. B. Borasoy, E. Epelbaum, H. Krebs, D. Lee, U.-G. Meißner, Eur. Phys. J. A **31**, 105 (2007) nucl-th/0611087.
55. E. Epelbaum, H. Krebs, D. Lee, U.-G. Meißner, Phys. Rev. Lett. **104**, 142501 (2010) arXiv:0912.4195 [nucl-th].
56. E. Epelbaum, H. Krebs, D. Lee, U.-G. Meißner, Phys. Rev. Lett. **106**, 192501 (2011) arXiv:1101.2547 [nucl-th].
57. E. Epelbaum, H. Krebs, T.A. Lähde, D. Lee, U.-G. Meißner, Phys. Rev. Lett. **109**, 252501 (2012) arXiv:1208.1328 [nucl-th].
58. T.A. Lähde, E. Epelbaum, H. Krebs, D. Lee, U.-G. Meißner, G. Rupak, Phys. Lett. B **732**, 110 (2014) arXiv:1311.0477 [nucl-th].
59. E. Epelbaum, H. Krebs, T.A. Lähde, D. Lee, U.-G. Meißner, G. Rupak, Phys. Rev. Lett. **112**, 102501 (2014) arXiv:1312.7703 [nucl-th].
60. B.N. Lu, T.A. Lähde, D. Lee, U.-G. Meißner, Phys. Rev. D **90**, 034507 (2014) arXiv:1403.8056 [nucl-th].
61. A. Gezerlis, I. Tews, E. Epelbaum, S. Gandolfi, K. Hebeler, A. Nogga, A. Schwenk, Phys. Rev. Lett. **111**, 032501 (2013) arXiv:1303.6243 [nucl-th].
62. A. Gezerlis, I. Tews, E. Epelbaum, M. Freunek, S. Gandolfi, K. Hebeler, A. Nogga, A. Schwenk, arXiv:1406.0454 [nucl-th].
63. T.D. Cohen, J.M. Hansen, Phys. Rev. C **59**, 13 (1999) nucl-th/9808038.
64. A.M. Gasparyan, M.F.M. Lutz, E. Epelbaum, Eur. Phys. J. A **49**, 115 (2013) arXiv:1212.3057 [nucl-th].
65. J.A. Oller, arXiv:1402.2449 [nucl-th].
66. V. Baru, E. Epelbaum, C. Hanhart, M. Hoferichter, A.E. Kudryavtsev, D.R. Phillips, Eur. Phys. J. A **48**, 69 (2012) arXiv:1202.0208 [nucl-th].
67. S. Ishikawa, M.R. Robilotta, Phys. Rev. C **76**, 014006 (2007) arXiv:0704.0711 [nucl-th].
68. V. Bernard, E. Epelbaum, H. Krebs, U.-G. Meißner, Phys. Rev. C **77**, 064004 (2008) arXiv:0712.1967 [nucl-th].
69. H. Krebs, A. Gasparyan, E. Epelbaum, Phys. Rev. C **85**, 054006 (2012) arXiv:1203.0067 [nucl-th].
70. V. Baru, C. Hanhart, M. Hoferichter, B. Kubis, A. Nogga, D.R. Phillips, Phys. Lett. B **694**, 473 (2011) arXiv:1003.4444 [nucl-th].
71. R.A. Arndt, R.L. Workman, M.M. Pavan, Phys. Rev. C **49**, 2729 (1994).
72. P. Büttiker, U.-G. Meißner, Nucl. Phys. A **668**, 97 (2000) hep-ph/9908247.
73. N. Fettes, U.-G. Meißner, Nucl. Phys. A **676**, 311 (2000) hep-ph/0002162.
74. J.M. Alarcon, J. Martin Camalich, J.A. Oller, Ann. Phys. **336**, 413 (2013) arXiv:1210.4450 [hep-ph].
75. Y.H. Chen, D.L. Yao, H.Q. Zheng, Phys. Rev. D **87**, 054019 (2013) arXiv:1212.1893 [hep-ph].
76. K.A. Wendt, B.D. Carlsson, A. Ekström, arXiv:1410.0646 [nucl-th].
77. M.C.M. Rentmeester, R.G.E. Timmermans, J.L. Friar, J.J. de Swart, Phys. Rev. Lett. **82**, 4992 (1999) nucl-th/9901054.
78. D.R. Entem, R. Machleidt, Phys. Rev. C **66**, 014002 (2002) nucl-th/0202039.
79. M.C.M. Rentmeester, R.G.E. Timmermans, J.J. de Swart, Phys. Rev. C **67**, 044001 (2003) nucl-th/0302080.
80. D.R. Entem, R. Machleidt, nucl-th/0303017.
81. A. Ekström, B.D. Carlsson, K.A. Wendt, C. Forssén, M. Hjorth-Jensen, R. Machleidt, S.M. Wild, J. Phys. G **42**, 034003 (2015) arXiv:1406.6895 [nucl-th].
82. R.N. Perez, J.E. Amaro, E.R. Arriola, arXiv:1411.1212 [nucl-th].
83. A. Ekstrom, G. Baardsen, C. Forssen, G. Hagen, M. Hjorth-Jensen, G.R. Jansen, R. Machleidt, W. Nazarewicz *et al.*, Phys. Rev. Lett. **110**, 192502 (2013) arXiv:1303.4674 [nucl-th].
84. J.R. Bergervoet, P.C. van Campen, W.A. van der Sanden, J.J. de Swart, Phys. Rev. C **38**, 15 (1988).
85. R.B. Wiringa, V.G.J. Stoks, R. Schiavilla, Phys. Rev. C **51**, 38 (1995) nucl-th/9408016.
86. R. Machleidt, Phys. Rev. C **63**, 024001 (2001) nucl-th/0006014.
87. T. Mehen, I.W. Stewart, M.B. Wise, Phys. Rev. Lett. **83**, 931 (1999) hep-ph/9902370.
88. E. Epelbaum, U.-G. Meißner, W. Glöckle, C. Elster, Phys. Rev. C **65**, 044001 (2002) nucl-th/0106007.
89. J.L. Friar, Phys. Rev. C **20**, 325 (1979).
90. V.G.J. Stoks, R.A.M. Klomp, C.P.F. Terheggen, J.J. de Swart, Phys. Rev. C **49**, 2950 (1994) nucl-th/9406039.
91. J.L. Forest, Phys. Rev. C **61**, 034007 (2000) nucl-th/9905063.
92. R. Machleidt, P. Liu, D.R. Entem, E. Ruiz Arriola, Phys. Rev. C **81**, 024001 (2010) arXiv:0910.3942 [nucl-th].
93. M.R. Schindler, D.R. Phillips, Ann. Phys. **324**, 682 (2009) **324**, 2051(E) (2009) arXiv:0808.3643 [hep-ph].
94. R.A. Arndt, I.I. Strakovsky, R.L. Workman, Phys. Rev. C **50**, 2731 (1994) nucl-th/9407035; SAID partial wave analysis online service, `http://gwdac.phys.gwu.edu/`.
95. D.R. Entem, N. Kaiser, R. Machleidt, Y. Nosyk, arXiv:1411.5335 [nucl-th].
96. M.C. Birse, J.A. McGovern, Phys. Rev. C **70**, 054002 (2004) nucl-th/0307050.
97. H.W. Grießhammer, Nucl. Phys. A **744**, 192 (2004) nucl-th/0404073.
98. H.W. Grießhammer, talk given at the *Workshop on Bound states and resonances in effective field theories and lattice QCD calculations, Benasque, Spain, July 20 - August 1, 2014.*
99. R.J. Furnstahl, D.R. Phillips, S. Wesolowski, J. Phys. G **42**, 034028 (2015) arXiv:1407.0657 [nucl-th].
100. C. van der Leun, C. Alderlisten, Nucl. Phys. A **380**, 261 (1982).
101. T.E.O. Ericson, M. Rosa-Clot, Nucl. Phys. A **405**, 497 (1983).
102. N.L. Rodning, L.D. Knutson, Phys. Rev. C **41**, 898 (1990).
103. A. Huber, T. Udem, B. Gross, J. Reichert, M. Kourogi, K. Pachucki, M. Weitz, T.W. Hansch, Phys. Rev. Lett. **80**, 468 (1998).
104. J. Martorell, D.W.L. Sprung, D.C. Zheng, Phys. Rev. C **51**, 1127 (1995).
105. D.M. Bishop, L.M. Cheung, Phys. Rev. A **20**, 381 (1979).
106. M. Kohno, J. Phys. G **9**, L85 (1983).
107. D.R. Phillips, J. Phys. G **34**, 365 (2007) nucl-th/0608036.

108. M. Piarulli, L. Girlanda, L.E. Marcucci, S. Pastore, R. Schiavilla, M. Viviani, Phys. Rev. C **87**, 014006 (2013) arXiv:1212.1105 [nucl-th].
109. H. Witala, J. Golak, R. Skibinski, K. Topolnicki, J. Phys. G **41**, 094011 (2014) arXiv:1310.0198 [nucl-th].
110. N. Fettes, V. Bernard, U.-G. Meißner, Nucl. Phys. A **669**, 269 (2000) hep-ph/9907276.
111. D. Siemens, V. Bernard, E. Epelbaum, H. Krebs, U.-G. Meißner, Phys. Rev. C **89**, 065211 (2014) arXiv:1403.2510 [nucl-th].
112. R. Navarro Perez, J.E. Amaro, E. Ruiz Arriola, Phys. Rev. C **88**, 064002 (2013) arXiv:1310.2536 [nucl-th].
113. W.P. Abfalterer, F.B. Bateman, F.S. Dietrich, R.W. Finlay, R.C. Haight, G.L. Morgan, Phys. Rev. C **63**, 044608 (2001).
114. G. Fink *et al.*, Nucl. Phys. A **518**, 561 (1990).
115. T.C. Montgomery *et al.*, Phys. Rev. C **16**, 499 (1977).
116. D.H. Fitzgerald *et al.*, Phys. Rev. C **21**, 1190 (1980).
117. R. Garrett *et al.*, Phys. Rev. C **21**, 1149 (1980).
118. A. Langsford *et al.*, Nucl. Phys. **74**, 241 (1965).
119. J.L. Romero *et al.*, Phys. Rev. C **17**, 468 (1978).
120. J. Wilczynski *et al.*, Nucl. Phys. A **425**, 458 (1984).
121. T.C. Griffith *et al.*, Proc. Phys. Soc. London Sect. A **71**, 305 (1958).
122. J. Rahm *et al.*, Phys. Rev. C **63**, 044001 (2001).
123. T. Rönnqvist *et al.*, Phys. Rev. C **45**, R496 (1992).
124. G.H. Stafford *et al.*, Lett. Nuovo Cimento **5**, 1589 (1957).
125. A.J. Bersbach *et al.*, Phys. Rev. D **13**, 535 (1976).
126. A.F. Kuckes *et al.*, Phys. Rev. **121**, 1226 (1961).
127. A.R. Thomas, D. Spalding, E.H. Thorndike, Phys. Rev. **167**, 1240 (1968).
128. Yu.M. Kazarinov *et al.*, SPJETP **16**, 24 (1963).
129. H.P. Stapp, T.J. Ypsilantis, N. Metropolis, Phys. Rev. **105**, 302 (1957).
130. J.M. Blatt, L.C. Biedenharn, Phys. Rev. **86**, 399 (1952).
131. J.M. Blatt, L.C. Biedenharn, Rev. Mod, Phys. **24**, 258 (1952).
132. C.M. Vincent, S.C. Phatak, Phys. Rev. C **10**, 391 (1974).